POSSIBILITIES AND LIMITATIONS OF CODED APERTURE IMAGING

A Thesis submitted
for the degree of
Doctor of Philosophy
by

RONALD LAKSHMAN SILVA

The University of Aston in Birmingham
Department of Physics

July 1981

DEDICATION

To the memory of my father;

to my mother,

Jenny, Pam, Anne and Tony

POSSIBILITIES AND LIMITATIONS OF CODED APERTURE IMAGING

RONALD LAKSHMAN SILVA

Doctor of Philosophy

Summary

We have simulated the performance of various apertures used in Coded Aperture Imaging - optically. Coded pictures of extended and continuous-tone planar objects from the Annulus, Twin Annulus, Fresnel Zone Plate and the Uniformly Redundant Array have been decoded using a noncoherent correlation process. We have compared the tomographic capabilities of the Twin Annulus with the Uniformly Redundant Arrays based on quadratic residues and m-sequences. We discuss the ways of reducing the 'd.c.' background of the various apertures used. The non-ideal System-Point-Spread-Function inherent in a noncoherent optical correlation process produces artifacts in the reconstruction. Artifacts are also introduced as a result of unwanted cross-correlation terms from out-of-focus planes. We find that the URA based on m-sequences exhibits good spatial resolution and out-of-focus behaviour when imaging extended objects.

Keywords

CODED APERTURE IMAGING; γ-RAY IMAGING; BIOMEDICAL IMAGING; TOMOGRAPHY; TWIN ANNULUS.

THE UNIVERSITY OF ASTON IN BIRMINGHAM

JULY 1981

LIST OF CONTENTS

LIST OF FIGURES

ACKNOWLEDGEMENTS

I would like to thank the following:

Professor G. L. Rogers for his guidance, encouragement and interest shown throughout the course of this work.

Professor S. E. Hunt in whose department this work was carried out and his advice on obtaining financial assistance.

The Science Research Council for providing the funds and making available the computing facilities at the Rutherford Computer Centre.

Dr. R. M. Vasu, my former colleague, for assistance in computer programming and for many lively discussions.

Howard Arrowsmith in the Physics workshop for advice on the design and construction of the apparatus and finally to Helen Turner for the efficient rendering of this thesis.

CHAPTER 1

HISTORICAL INTRODUCTION

CHAPTER 1

HISTORICAL INTRODUCTION

Historically, the Freznel Zone Plate (FZP) was the first coded aperture or aperture code to be used in imaging since its connection with holography was realised by Rogers[1-4]. The pioneering work was done by Mertz and Young[5] when they substituted a FZP for a pinhole in their X-ray camera, used in Stellar photography. The coded picture was termed a noncoherent hologram[1] since its formation depended on a FZP, noncoherent light and geometrical optics.

Each point on a self-luminous object is considered to cast a shadow of the FZP onto the image plane. Object points at different distances from the FZP will cast shadows of different scales. Thus, this ensemble of FZPs is termed a noncoherent hologram. The whole process is sometimes referred to as shadow holography.

Several authors[7-25] have formed these noncoherent holograms using X-rays and γ-rays. One of the reasons for using a coded aperture such as a FZP was to investigate the possible improvement (if any) in the signal-to-noise ratio (SNR) of the reconstructed object. Thus a coded aperture system needed to maintain the high angular resolution of a single pinhole camera whilst increasing the photon count on the detector plane. The many openings of a coded aperture, although increasing the count rate, does not in

itself guarantee an improved SNR. The possible improvement depends on the object, the pattern of openings in the coded aperture and the processing techniques used. A coded aperture imaging system also offers the possibility of tomography.

Rogers[26] noted that the process of in line holography of Gabor was equivalent to correlating the noncoherent hologram with a complex-phase zone plate. Mertz and Young[5] used this 'in-line' technique to recover the object. Thus, the hologram was formed with noncoherent light and reconstructed in coherent light. Difficulties associated with 'twin images' in Gabor in line holography were overcome by Young[6] and Barrett et al.[8] with the adoption of an off-axis FZP as the coded aperture, analogous to the off-axis holography of Leith and Upatnieks[27].

It should be mentioned at this point that the formation of noncoherent holograms and their subsequent decoding were successful only in the case of 'dilute' objects. That is objects which are almost entirely black, with relatively few patches of illumination on the background[28]. Lingren et al.[17] have estimated that a dilute object occupying 5% of the available field has a good chance of recovery with a FZP.

However, Barrett et al.[8] have used the off-axis FZP to form noncoherent holograms of continuous-tone objects. This was achieved by modulating the object with a grating

so that the object's spatial frequencies were projected onto the pass band of the off-axis FZP. The best results have been obtained using this technique. Reconstructions are of course achieved in coherent light.

Silva and Rogers[19] have shown that in the case of dilute objects, the image could be recovered if the noncoherent hologram is correlated with the original FZP code, in a noncoherent correlator. The contrast however, is very poor. This method is consistent with the Gabor in line technique where the complex phase zone plate is replaced by an amplitude FZP. In this text the term noncoherent hologram will only be used when referred to FZP imaging.

Considerable work has been done by several authors using random dot codes or random arrays[29-32]. Dicke[29], the pioneer of this type of code, was concerned with continuous tone objects and concluded that to record more than 100 equally intense point sources a coded aperture of 10^6 holes were required. Unequal intensities of the object produced further limitations. For instance, if they were only two sources, an intensity ratio of 100:1 is the limit of detection.

Alquazzaz and Rogers[32] have proposed that the central peak in the autocorrelation of the code, is an adequate guide to the degree of recovery likely to occur in the case of continuous tone objects. They have suggested drawing

a circle, which they call the signal-to-noise ratio circle or SNR circle, that encloses half the N(N-1) dots of the code on the shoulder of the autocorrelation pattern. Thus some points of the object will contribute to the SNR circle while others do not. Extreme points will tend to contribute more to the shoulder. Hence, the SNR circle may be a little smaller than the original code, but recovery due to correlation between output (coded picture) and original code is not very great.

Akcasu et al.[33,34], Macovski[35] and Koral et al.[36] have used digital techniques to recover the image from a coded picture formed by a time-modulated random pinhole code. They have devised a method of minimising noise due to cross correlation terms which are not quite uniformly distributed in frequency space. This is achieved by moving a random hole mask across a limiting aperture in a number of steps during the exposure. At present, the procedure is time consuming.

Other workers have used the nonredundant array (NRA) to form a coded picture of the object[37-42]. Klotz and Weiss[39] produced their X-ray pictures using a NRA of 10 tubes. The coded picture is built up by overlapping a number of different viewpoints. Reconstruction is achieved by performing a whole series of correlations, using the basic code pattern (NRA) at various scales. Again, this procedure works well with dilute objects. Klemperer[41] has described one of the largest NRAs known.

This has 24 holes and a density of only 0.03 (i.e. the ratio of the open area of an aperture to the total area). However, the small number of holes means that in non-coherent optical processing, the SNR over a pinhole will not be increased appreciably. A coded aperture technique combined with noncoherent optical processing for the particular case of a point source object, will offer an improvement in the SNR of the order of $\sqrt{N}$, where N is the number of degrees of freedom in the illuminating beam transmitted by the optical system[43].

The use of an Annulus as a coded aperture has also attracted many workers[44-50]. The decoding of the coded pictures has been performed electronically, digitally, by coherent optical means and by noncoherent optical correlation[50]. A variant of the Annulus and FZP called the Twin Annulus has also been presented as a new aperture by Silva and Rogers[50].

A major contributing factor to the degree of recovery of an object is noise. In γ-ray imaging it is the shot noise that arises from the particular nature of the photons used. Statistical fluctuations in the number of γ-rays arriving at the detector in a reasonable recording time produces shot noise, resulting in a grainy or speckly image. The presence of shot noise imposes distinct limits on the product of resolving power by field size.

Rogers et al.[12], assuming a photographic record,

thereby equating the grain noise in the film to the photon shot noise in the detector, have worked out the noise effects for a pinhole camera, using a narrow aperture in a lead shield. They have shown, as Haine and Mulvey[51] did, that the noise increases as the square of the number of resolved points as the latter is increased in the object. Thus if the number of resolved points in an object is M, then the noise goes up as M^2 for noncoherent holography whilst it goes up as M for coherent holography.

Barrett and Horrigan[15], by considering the increase in photon count necessary to maintain a given SNR as the resolving power is increased at constant field size, arrived at a similar result. They conclude that for a pinhole and a FZP the count rate must go up as d^{-4} where d is the resolution distance. The number M of resolved points in the field goes up as d^{-2} so that the counts (n) must go up as the square of this keep the statistical fluctuations, proportional to $n^{\frac{1}{2}}$ to a steady level.

Lingren et al.[17] have analysed the problem of noise in FZP and pinhole imaging by considering the 'dilution' of the object. They assume the detector to be ideal and the noise to be signal-independent and conclude that the FZP is superior to pinhole methods if the proportion of occupied sites is less than 5%.

Brunol and Fonroget[47] have shown that the noise depends on the type of code used. They have found that the

SNR for an annulus is much better than that for a FZP of the same resolution and dimension for high spatial frequencies. However, for very low spatial frequencies the reverse is true. Decoding is achieved via linear filtering techniques similar to Wiener filtering.

Recently, Fenimore and Cannon[52-56] have proposed the use of a uniformly redundant array (URA), derived from a class of pseudonoise array[57,58] in coded aperture imaging[25,59]. These have the desirable property of a uniform shoulder in the system-point-spread function (SPSF) which can be subtracted by digital correlation techniques. Fenimore[53] has predicted that the URA will always give a better image than that from a single pinhole in the case of a few (10 to 20) point sources.

We shall be comparing the performances of the FZP, Annulus, Twin Annulus and URA as coded apertures when imaging extended objects using a noncoherent optical correlation system of decoding. We also compare the tomographic capabilities of the URA and Twin Annulus when subjected to this decoding system. We discuss the relative merits of a noncoherent optical approach to processing coded aperture imaging in the next chapter.

CHAPTER 2

NONCOHERENT OPTICAL PROCESSING

CHAPTER 2

NONCOHERENT OPTICAL PROCESSING

The existence of a Fourier transform relation between the front and rear focal planes of a lens, when coherent illumination is used, forms the basis of many coherent optical processing systems[60.-66]. Because of this Fourier transform relationship, operations can be performed in the spatial frequency domain. Hence, an analogy can be drawn with electrical filters; and spectrum analysis, pattern recognition and image processing become possible optically.

However, a noncoherent optical processing system does not have a Fourier transform plane and the above operations are performed in the spatial domain. A review of such optical correlators is given by Monahan et al.[67]. The basic principles of noncoherent optical processing is described by Rogers[68, 69]. The presence of redundancy[70], R, in a noncoherent system lends itself to a high resistance to noise.

$$R = \frac{\text{Information}^{*} \text{ carrying capacity of system}}{\text{Information actually being carried}}$$

Because of the diffuseness of the object in a noncoherent optical processing system, it can be regarded as a communications system with a large number of channels carrying the same information in parallel. Assuming a Lambertian

* Information = Etendu/λ^2

source, essentially the same information about the source is beamed out over a central region of at least $\pm 20^{\circ}$, hence its resistance to noise[68,69]. It is well known that coherent systems, which are frequently nonredundant, are easily upset by the presence of dust or small disturbing particles.

Chavel and Lowenthal[43] have studied the influence of coherence on noise in an optical image and characterised it into two main kinds: the setup noise (pupil noise) and the input noise. They show that there is a definite advantage in using noncoherent light instead of coherent, as far as setup noise is concerned. The gain in SNR is then of the order of $\sqrt{N}$, where N is the number of degrees of freedom in the illuminating beam transmitted by the optical system. This gain increases with increasing illuminating aperture upto a maximum reached when the latter is equal to the imaging aperture, then the gain remains constant. For input noise (impulse noise or granularity noise in the object) there is no significant difference between coherent and noncoherent illumination, except for phase noise. Therefore, the main advantage of using noncoherent illumination as far as the input noise is concerned is the suppression of phase noise. They find that due to the Callier effect, the image contrast is a maximum when the illuminating aperture equals the imaging aperture.

The use of noncoherent optical processing techniques

in obtaining for example correlation and convolution functions as opposed to an electronic approach is two-fold. Firstly, a noncoherent optical system performs a linear mapping on functions of two independent variables compared with the single variable of time in an electronic system. In addition, this mapping of the two independent variables takes place simultaneously. Considering that good quality lenses have a space-bandwidth product of over 10^7, this represents a powerful parallel processing capacity. Secondly, analog multiplications are determined by input and output rates. There is of course the question of comparative cost. The heart of a noncoherent optical processing system is a diffuse source.

The major drawback on noncoherent optical processing is that it works with luminous intensities and intensities can only be added. Thus it is not possible to represent directly, a bipolar function. Such functions have to be transformed into a positive function by adding a d.c. bias term[68,69].

The main advantages of a noncoherent optical processing system are a combination of redundancy, parallel processing and a very high resistance to noise.

CHAPTER 3

MATHEMATICAL PRELIMINARIES

CHAPTER 3

MATHEMATICAL PRELIMINARIES

3.1 DEFINITIONS

The operation of a noncoherent optical system can be described by a general linear transformation of the form:

$$g(p) = \int f(x)h(x;p)dx \qquad (3.1.1)$$

in the one-dimensional form or

$$g(p,q) = \iint f(x,y)h(x,y;p,q)dxdy \qquad (3.1.2)$$

in the two-dimensional form. (The limits of integration are determined for each particular transformation). In general f(x) is termed the input function

h(x;p) the impulse response function, see Fig. 3.1.1.

Fig. 3.1.2 lists a few examples of linear transformations performed optically. Thus a two dimensional convolution may be written as:-

$$C_{fh}(p,q) = \iint f(x,y)h(p-x,q-y)dxdy \qquad (3.1.3)$$

and a two-dimensional cross-correlation as

$$\varphi_{fh}(p,q)=\iint f(x,y)\,\bar{h}(x+p,y+q)dxdy \qquad (3.1.4)$$

and a two dimensional Autocorrelation as

$$\varphi_{ff}(p,q)=\iint f(x,y)f(x+p,y+q)dxdy \qquad (3.1.5)$$

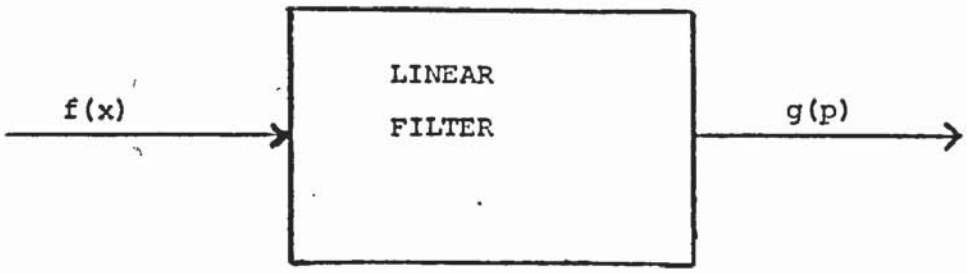

Fig. 3.1.1 Linear Transformations

General linear filter characterised by the impulse response h(x;p). The input f(x) is transformed into the output g(p) through a linear transformation integral.

Transformation	Impulse response function
Convolution	$h(p-x)$
Cross correlation	$h(x+p)$
Autocorrelation	$f(x+p)$

Fig.3.1.2 Examples of linear transformations

Some commonly used transformations in signal processing systems. Each transformation is of the form Eqn.3.1.1 with respective impulse response functions $h(x;p)$.

For convenience and brevity we will represent the correlation integral by the symbol * and the convolution integral by the symbol $\circledast$.
Thus we represent convolution by:

$$C_{fh}(p,q) = f(x,y) \circledast h(x,y) \qquad (3.1.3a)$$

Cross-correlation by:

$$\varphi_{fh}(p,q) = f(x,y) * h(x,y) \qquad (3.1.4a)$$

Autocorrelation by:

$$\varphi_{ff}(p,q) = f(x,y) * f(x,y) \qquad (3.1.5a)$$

3.2 PRINCIPLE OF LINEAR SUPERPOSITION

Let us now consider the principle of linear superposition in optical image formation as elucidated by E. L. O'Neill[71].

It is proposed that an optical image can be considered to be a linear superposition of impulse responses (PSFs) integrated over the entire object plane. See Fig. 3.2. For simplicity we make the following assumptions. The magnification is unity; the light from the object is noncoherent; the distribution of light at (p,q), due to the point source of light at (x,y) is given by h(p-x,q-y), i.e. the system is linear; and that this distribution does not change as we explore the field, i.e. the system is space invariant.

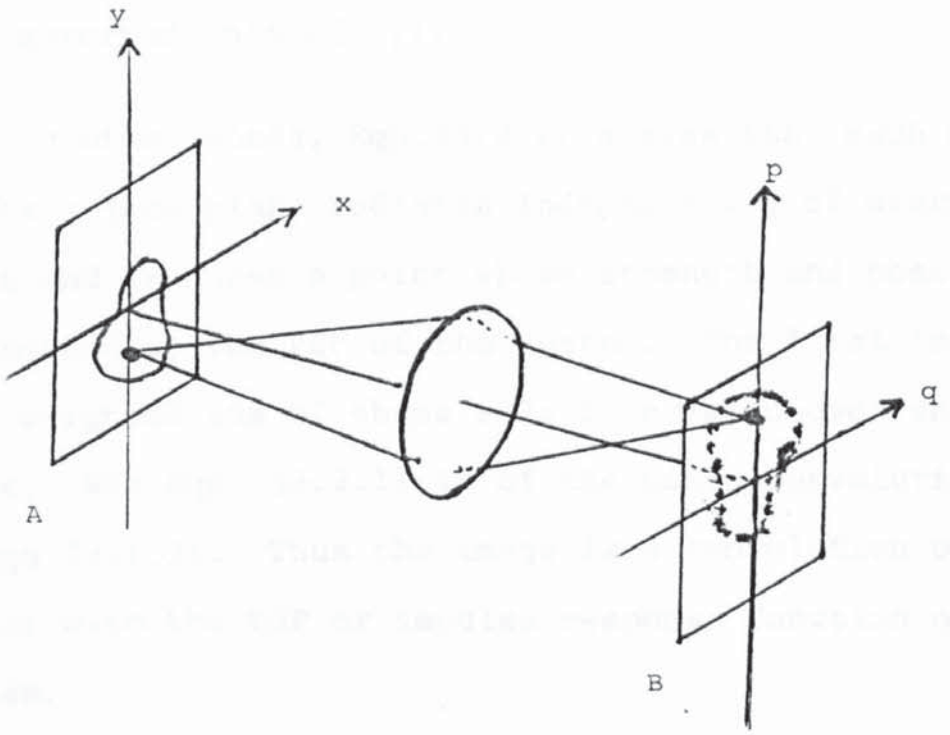

$$I(p,q) = \int_{-\infty}^{+\infty}\int O(x,y)\ h(p-x,q-y)\ dxdy$$

Fig. 3.2.1 The principle of Linear Superposition.

An optical image can be considered to be a linear superposition of PSFs integrated over the entire object plane,A. The image plane is B. O(x,y) and I(p,q) are the brightness of the object and image respectively..

Then if O(x,y) describes the brightness of the object and I(p,q) the brightness of the image we get:-

$$I(p,q) = \int\int_{-\infty}^{+\infty} O(x,y)h(p-x,q-y)dxdy \qquad (3.2.1)$$

where the actual limits on the size of the object have been absorbed into O(x,y).

In other words, Eqn.(3.2.1) states that each point in the object plane radiates independently of every other point and produces a point whose strength and position is determined by the PSF of the system. The final image is a weighted sum of these PSFs integrated over the object plane. Now Eqn. (3.2.1) is of the basic convolution form see Eqn (3.1.3). Thus the image is a convolution of the object with the PSF or impulse response function of the system.

$$I(p,q) = O(x,y) \circledast h(x,y) \qquad (3.2.2)$$

3.3 CODED PICTURE FORMATION

Fig. (3.3.1) shows the basic setup in forming the coded picture. O(x,y) is the object transparency which is placed in contact with an extended diffuse source. For the purpose of analysis it is assumed that the extended diffuse source obeys Lamberts Law. That is, one for which the flux* at an angle θ to the surface normal falls off as cos θ. It can be shown that for

*flux is the luminous power emitted into a small solid angle per unit solid angle.

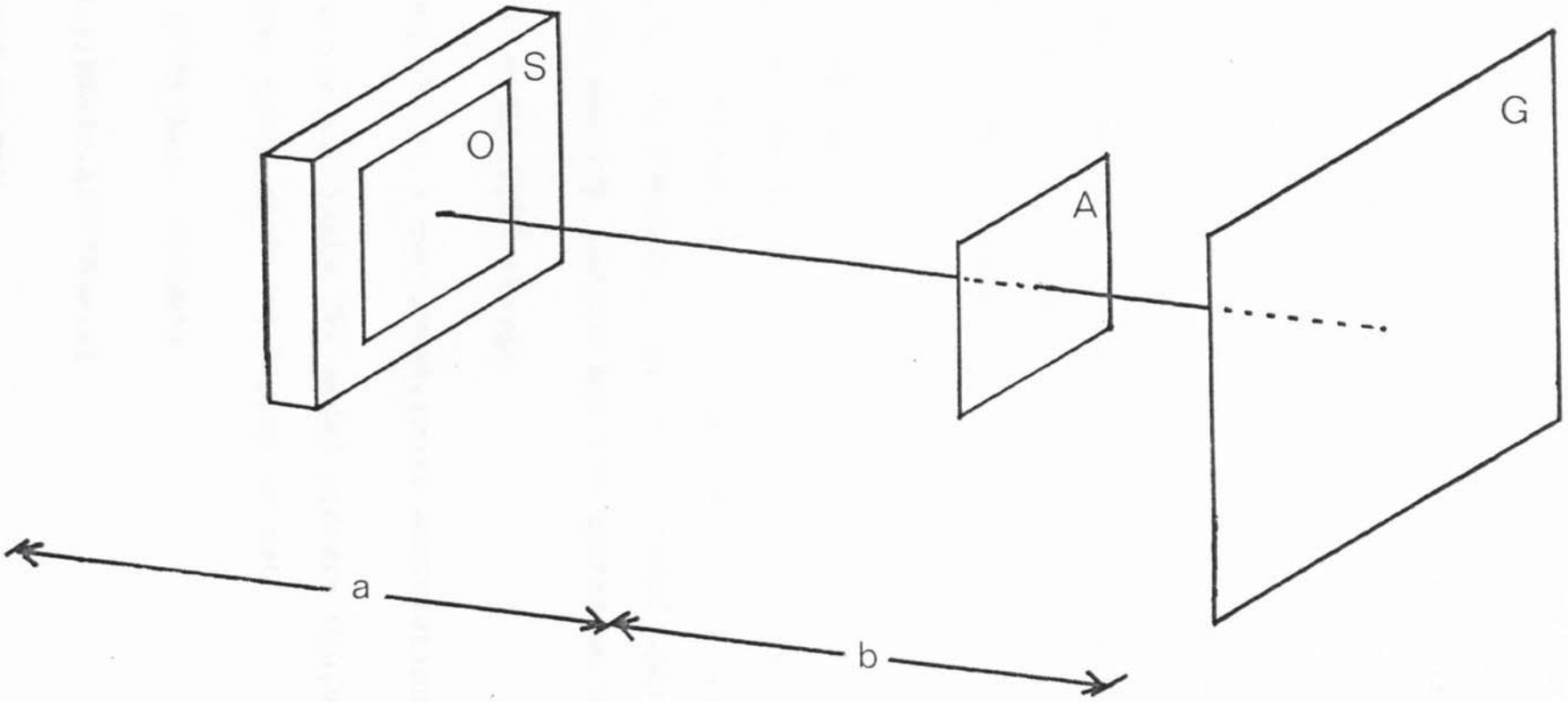

Fig. 3.3.1 Geometry of coded picture formation.
S- Diffuse source, O- Object plane, A- coded aperture plane, G- convolution plane.
a- object to coded aperture distance
b- coded aperture to coded picture distance

such a surface an angle of $\pm 20^{\circ}$ to the normal has a fall-off in intensity of only 6%, which is not of much practical importance. The presence of the object transparency in contact with the source produces a variation which is now a function of the source coordinates. It alters the scale of the polar diagram and modifies its shape due to the presence of increased photographic density, to oblique rays.

The coded aperture A(p,q) is placed at a distance 'a' from the plane of the object. The detector, in our case photographic film is placed at a distance 'b' from the coded aperture.

If the system is linear, space-invariant and limiting ourselves to planar objects, the coded picture G(u,v) is a convolution of the object O(x,y), suitably scaled, with the intensity PSF of the coded aperture. Omitting the scaling factors for the moment we can write

$$G(u,v) = O(x,y) \circledast\circledast A(p,q) \qquad (3.3.2)$$

where $\circledast\circledast$ signifies a two-dimensional convolution.

If we now correlate the coded picture G(u,v) with the original coded aperture A(p,q) we get

$G(u,v) ** A(p,q)$ becomes

$\{O(x,y) \circledast\circledast A(p,q)\} ** A(p,q)$

re-arranging we get

$\{A(p,q) ** A(p,q)\} \circledast\circledast O(x,y)$

thus we can recover $O(x,y)$ if and only if

$$\{A(p,q)**A(p,q)\}\rightarrow \delta(x,y)$$

where δ is the Dirac delta function.

So, the autocorrelation of the coded aperture must be a delta function. However, this need not be the case if we can find a different function which when correlated with the coded aperture will yield the desired delta function. Let this function be $B(p,q)$, then correlating the coded picture with $B(p,q)$ we get

$$G(u,v)**B(p,q)$$

i.e. $$\{O(x,y)\circledast\circledast A(p,q)\}**B(p,q)$$

$$\{A(p,q)**B(p,q)\}\circledast\circledast O(x,y)$$

thus we require

$$\{A(p,q)**B(p,q)\}\rightarrow\delta(x,y)$$

Let us now consider a geometrical approach to the formation of a coded picture. Now,

$$G(u,v)=(\frac{b}{a})O(x,y)\circledast\circledast(\frac{a+b}{a})A(p,q) \qquad (3.3.3)$$

If the coded aperture is centro-symmetric, then Eqn (3.3.3) is also a two-dimensional correlation.

Let d and D be the diameters of the object and code respectively. Fig. (3.3.2). Let θ by the angle made by an

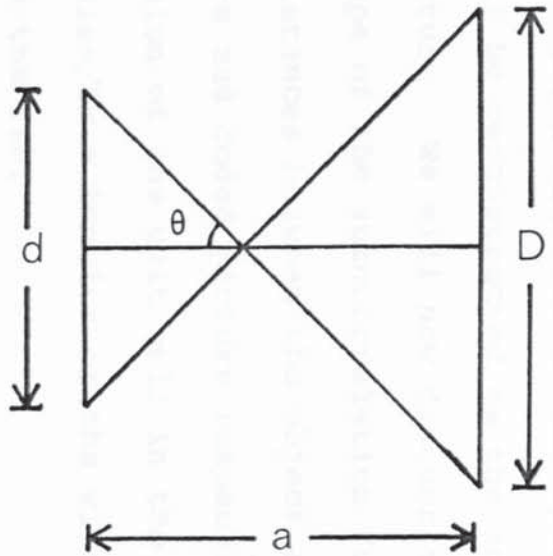

Fig. 3.3.2 Lambertian intensity variation over the object field.

d- diameter of object, D- diameter of coded aperture,
θ- angle made by off axis ray to the normal.

off-axis ray with the normal. Now,

$$\theta = \tan^{-1}\left(\frac{D+d}{2a}\right) \tag{3.3.4}$$

The intensity fall-off from Lambert's law is proportional to $\cos^4\theta$. Since our reconstruction technique involves a reversal ray method, viz. correlating the coded picture with the original coded aperture, the overall intensity fall-off, I_o, becomes proportional to $\cos^8\theta$.

$$\text{i.e. } I_o \alpha \left|1 + \left(\frac{D+d}{2a}\right)^2\right|^{-1} \tag{3.3.5}$$

Ideally, 'a' must be large compared to (D+d) to minimise I_o.

The resolving power of a coded aperture can be derived from the autocorrelation function of the aperture. A point source object will be reconstructed as the autocorrelation of the coded aperture. We will now discuss the factors effecting the shape of the autocorrelation function. Let a and b be the distances between the object and coded aperture and coded aperture and coded picture respectively. Let w be the linear dimension of the unit cell in the URA or the width of the Annulus/Twin Annulus or the width of the outermost zone in the FZP.

Consider for simplicity a disc object represented by its diameter d. On the convolution plane we have d scaled by a factor $(\frac{b}{a})$. See Eqn. (3.3.3). Therefore,

$$d_u = d\left(\frac{b}{a}\right) \tag{3.3.6}$$

where d_u is the projected diameter on the convolution plane. Now, the intensity PSF of the coded aperture will be scaled to $D(\frac{a+b}{a})$ and in particular the width of the coded aperture w, on the convolution plane denoted by w_u will be given by:

$$w_u = w(\frac{a+b}{a}) \tag{3.3.7}$$

If $d_u=w_u$ then the object is said to be"matched" with the code, i.e. the object and aperture shadows are equal in size. Barrett and Horrigan[15] proposed the same condition for the frequency matching condition for FZPs. When $d_u=w_u$ we get

$$d = w(\frac{a+b}{b}) \tag{3.3.8}$$

where d is the minimum resolvable distance of the object. Re-writing Eqn. (3.3.8.) we get

$$d_{(min)} = w(1+a/b) \tag{3.3.9}$$

If $d_{(min)}$ is the minimum resolvable distance in the object, then it should be the diameter of the autocorrelation peak. Thus, for a fixed aperture width w, the diameter of the autocorrelation peak increases as (a/b) increases. When a=b, $d_{(min)}=2w$ and it is evident that $d_{(min)}\neq w$ and will always be greater than w.

Ideally, w should be small as possible. We see that from Eqns. (3.3.5) and (3.3.9) that 'a' must be large to

avoid biasing the object with an intensity fall-off and that 'a' must be small to reduce the diameter of the autocorrelation peak and hence have a small resolvable distance. We shall now consider the effect of diffraction on the choice of w. Our analysis up to now has been under the assumption of diffractionless optics.

Using the Fresnel half period zone criterion we can see that we confine ourselves to the geometrical region, providing the aperture width w is greater than the radius of the Fresnel half period zone r.

$$\text{where } r^2 = \left(\frac{ab}{a+b}\right)\lambda \qquad (3.3.10)$$

and λ is the wavelength of radiation used so to be within the geometrical region $w>r$. Hence, $d_{(min)}$ is a function of a, b and λ. It can be seen from Eqns. (3.3.9) and (3.3.10) that we have to accept a certain amount of intensity fall-off over the object field in order to extend the resolution of the system.

CHAPTER 4

OPTICAL IMPLEMENTATION OF CORRELATIONS AND CONVOLUTIONS

CHAPTER 4

OPTICAL IMPLEMENTATION OF CORRELATIONS AND CONVOLUTIONS

4.1 COHERENT PROCESSORS

A typical coherent optical processor involves making a holographic filter and is subject to serious noise problems. Fig. 4.1.1 shows a scheme which can be used with either coherent or noncoherent illumination. The input masks A and B must be placed in contact with each other and placed between the lenses C and L. Thus the masks are illuminated by a coherent parallel beam of light. The function B (say) is scanned across the function A and the correlation function is obtained sequentially from the detector output D.

If A is a function $f(x,y)$ and B the same function displaced a distance p in the x-direction and q in the y-direction, with A and B in contact. Then the autocorrelation function in two dimensions

$$\varphi_{ff}(p,q) = \frac{1}{ab} \int_0^a \int_0^b f(x,y) f(x+p,y+q)\,dx\,dy \qquad (4.1.1)$$

is calculated in a sequential manner.

First, the product of the two functions is performed and the lens L projects this composite function onto a photocell. This gives a single value of φ_{ff} for one pair of values p and q. We must build up φ_{ff} successively by scanning B over all desired values of p and q. However, the factor $(\frac{1}{ab})$ is not calculated.

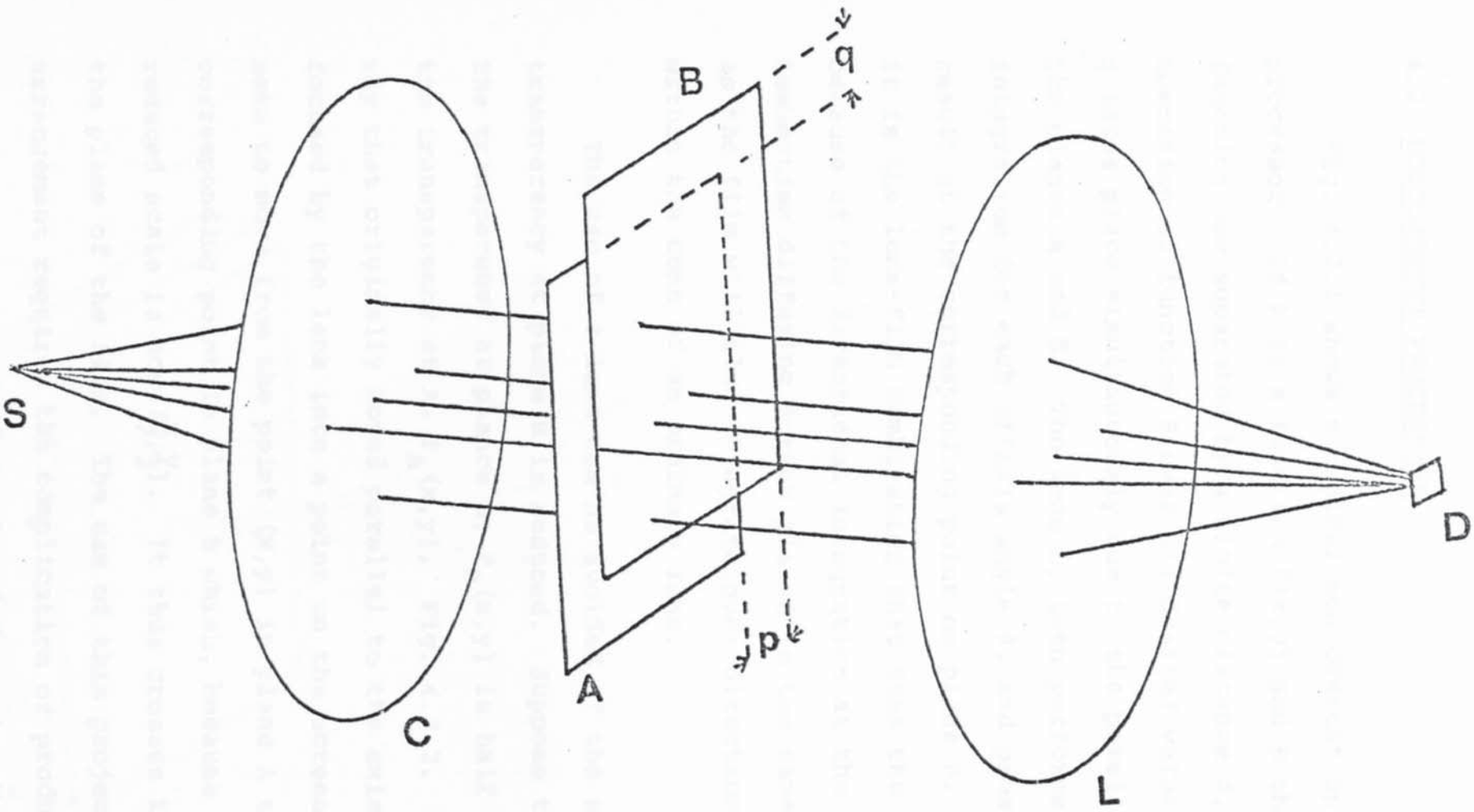

Fig. 4.1.1 The Coherent Correlator.

S= coherent source

C= collimator

L= focusing lens

D= photodetector

A and B are the input masks placed in contact with each other

4.2 NONCOHERENT PROCESSORS

Fig. 4.2.1 shows a typical noncoherent optical processor. If A is a function f(x,y) and B the same function now separated by a finite distance d, the scanning operation of function B over all desired values of p and q takes place simultaneously due to the parallax between the planes A and B. The lens L, then performs the integration for each offaxis angle θ, and presents the result at the corresponding point on plane P. More strictly, it is the lens-film combination that does the integration, because of the directional integration at the film. A Lambertian diffusing screen placed in the same position as the film will also integrate over direction, at least within the cone of an ordinary lens.

The use of a lens can be avoided if the scale of the transparency at plane B is reduced. Suppose the scale of the transparency at plance B, $f_B(x,y)$ is half the scale of the transparency at A, $f_A(x,y)$, Fig. 4.2.2. Then the ray that originally moved parallel to the axis and was focused by the lens into a point on the screen P, is now seen to move from the point (x,y) in plane A to the corresponding point in plane B which, because of the reduced scale is now $(\frac{x}{2},\frac{y}{2})$. It thus crosses the axis in the plane of the film. The use of this projective arrangement requires the complication of producing correctly scaled transparencies $f_A(x,y)$ and $f_B(x,y)$. However, it

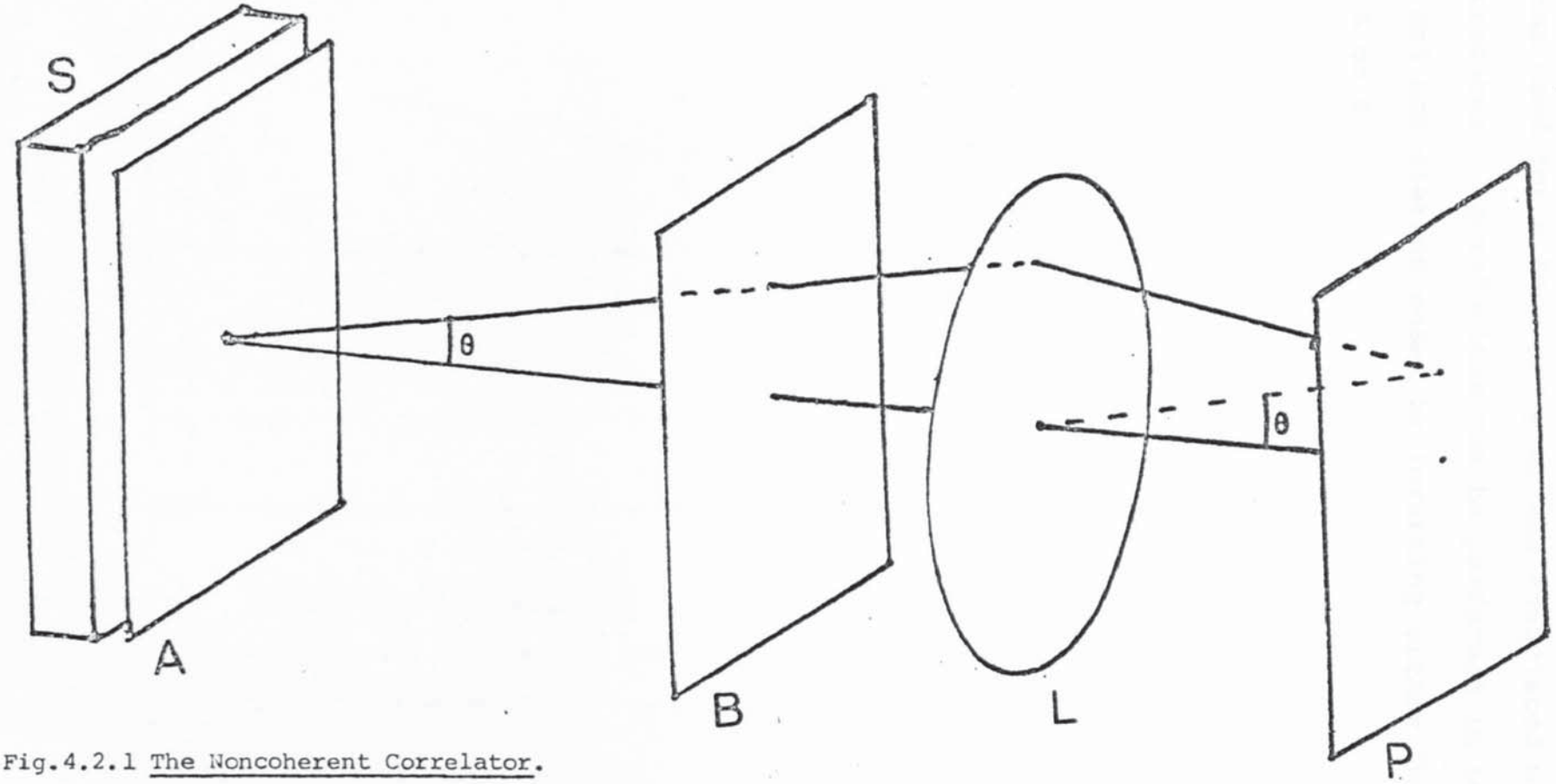

Fig.4.2.1 The Noncoherent Correlator.

S= diffuse source; A and B are input masks separated by a finite distance d ; L = lens;
P= plane of film or diffuse screen

removes the need for a lens and problems associated with lens aberrations. Convolutions can be performed in both coherent and noncoherent cases by inverting either function in plane A or B.

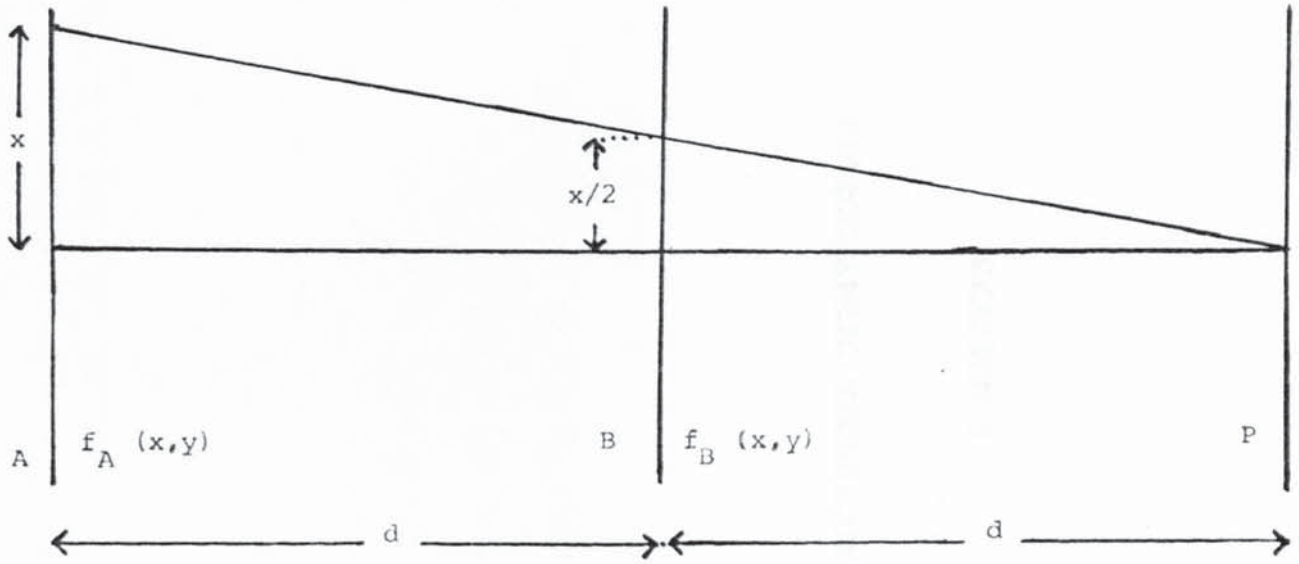

Fig. 4.2.2 Correlation without a lens.

f_A (x,y) and f_B (x,y) are transparencies at plane A and B respectively.
P is the plane of the screen.

CHAPTER 5

PHOTOGRAPHIC TECHNIQUE

CHAPTER 5

PHOTOGRAPHIC TECHNIQUE

5.1 DEFINITIONS

5.1.1 Transmission

The transmission T, of an area of negative is defined as the ratio of the light transmitted, I_t, to the incident light on the negative, I_i. It is expressed as

$$T = \frac{I_t}{I_i} \tag{5.1.1}$$

Transmission is always less than unity and is normally expressed as a percentage.

5.1.2 Opacity

Opacity, O is defined as the ratio of the light incident on the negative, I_i, to the light transmitted, I_t. It is expressed as

$$O = \frac{I_i}{I_t} \tag{5.1.2}$$

It is apparent that

$$O = \frac{1}{T} \tag{5.1.3}$$

and is always greater than unity.

5.1.3 Density

The density, D, is defined as the logarithm of the

opacity O. That is

$$D = \log O = \log\left(\frac{1}{T}\right) = \log\left(\frac{I_i}{I_t}\right) \qquad (5.1.4)$$

5.1.4 Exposure

The exposure, E, is defined as the product of incident illumination, I_i, and exposure time t. That is

$$E = It \qquad (5.1.5)$$

It is expressed in lux seconds. (lux is the luminous power per unit area incident on a surface).

5.1.5 The Characteristic Curve

If density, D, as ordinate is plotted against exposure, E, as abscissa, a response curve for a film or plate of the general shape shown in Fig. 5.1.1 is obtained. However, a far more useful curve is obtained by plotting density, D, against log(exposure), LogE as in Fig. 5.1.2. This curve is referred to as the characteristic curve or H and D curve. For convenience, the characteristic curve is divided into four main sections: the toe; an approximately straight-line portion; the shoulder, and the region of solarisation. Provided the density and logE axes are equally scaled, the numerical value of the tangent of the angle, θ, which the straight line portion of the curve makes with the logE axis, is termed gamma, γ. It is seen that γ serves to measure contrast, i.e. the rate at which density grows as log exposure increases, in the straight line portion of

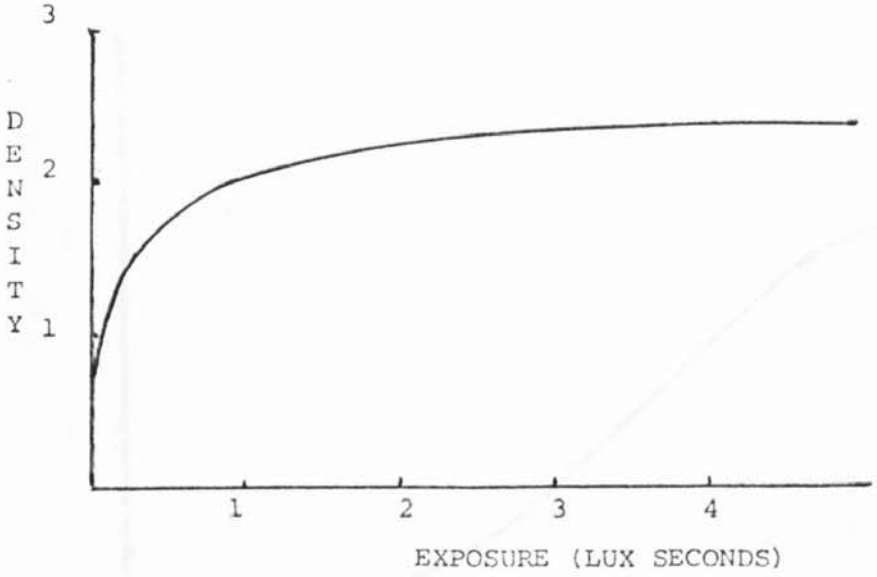

Fig. 5.1.1 Response curve of a photographic film plotting density versus exposure.

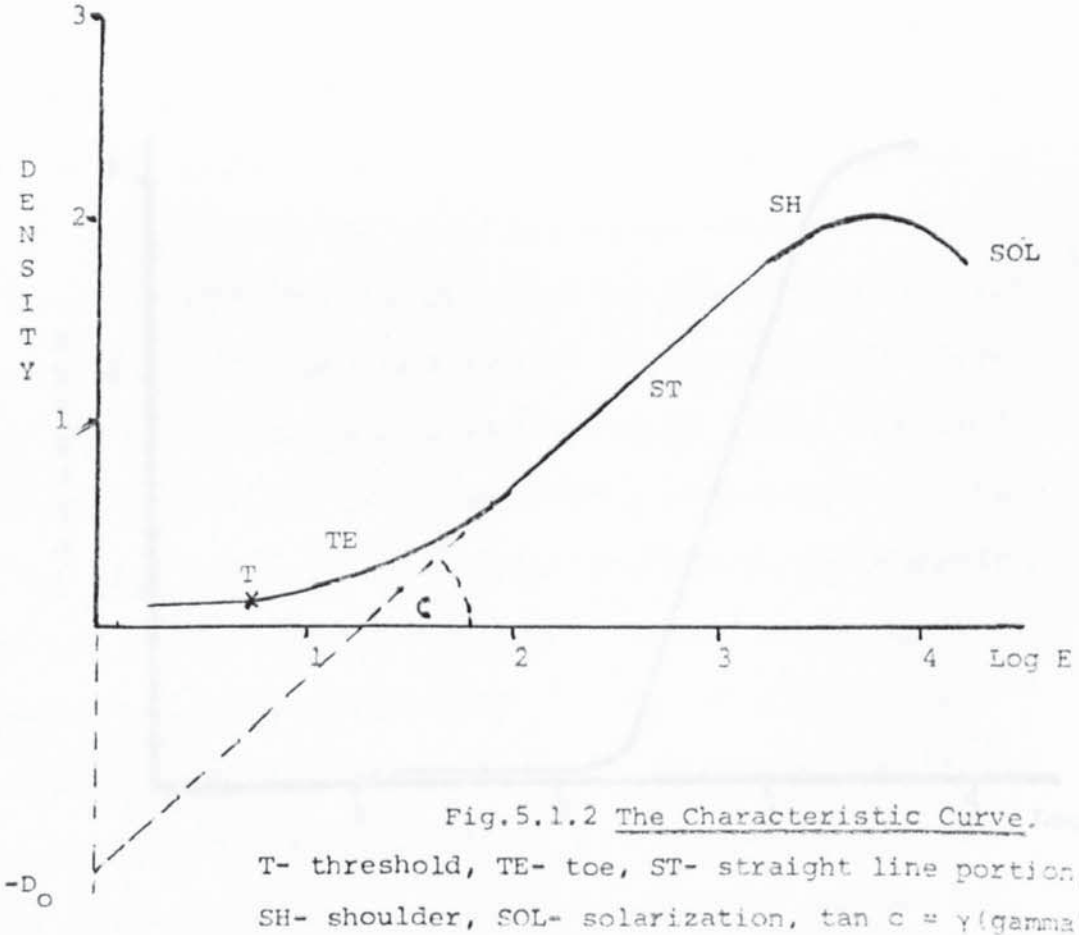

Fig.5.1.2 The Characteristic Curve.

T- threshold, TE- toe, ST- straight line portion, SH- shoulder, SOL- solarization, tan c = γ(gamma).

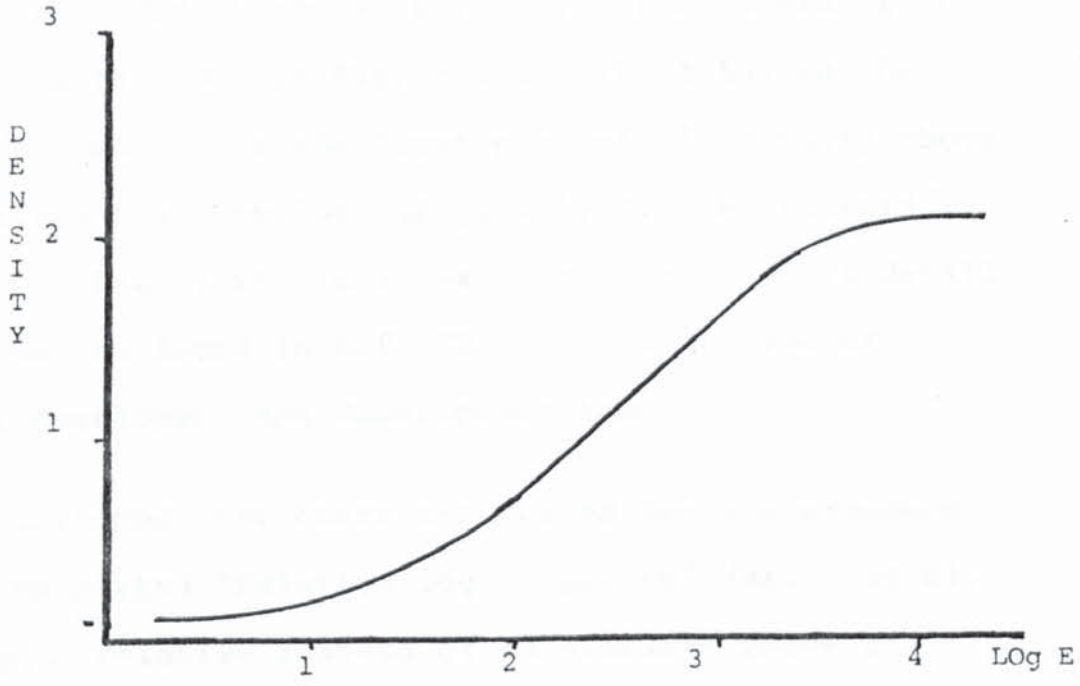

Fig. 5.1.3 The Characteristic Curve for a low gamma film.

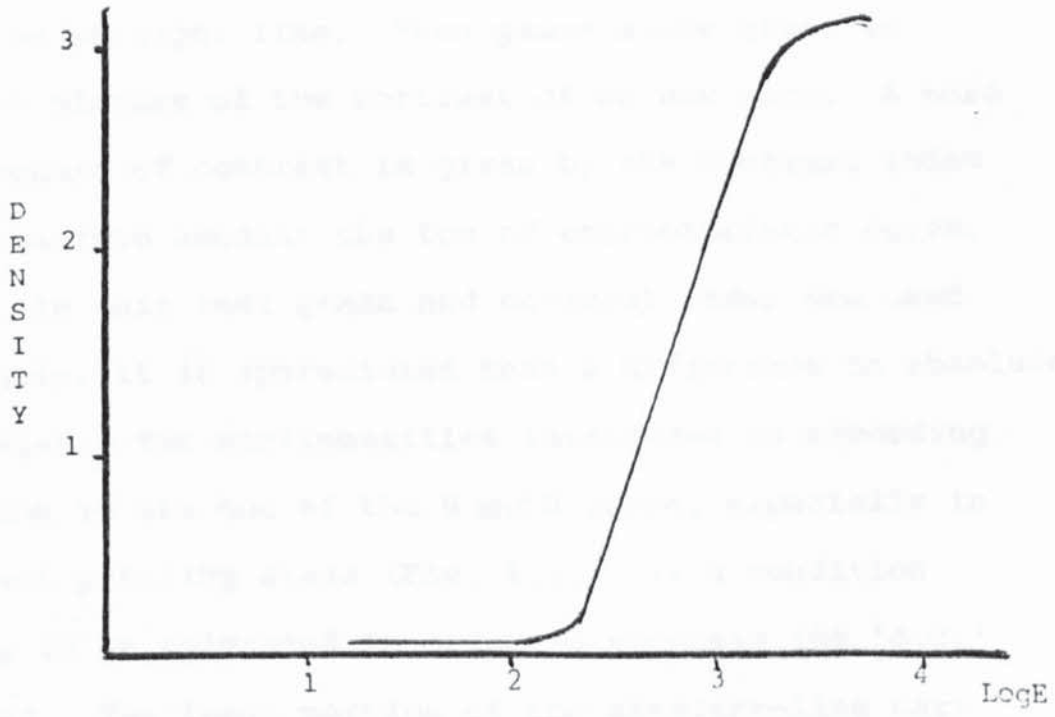

Fig. 5.1.4 The characteristic Curve for a high gamma film.

of the curve. The characteristic curve for Ilford ortho (SP343) film is shown in Fig. 5.1.3.. The point on the curve corresponding to the first perceptible density above fog is called the threshold (Fig. 5.1.2).. The factors which effect film γ will only be listed here. More detail analysis may be found in Ref. 72. They are: type of emulsion; developer; and development time.

On published characteristic curves the log exposure axis may be marked "relative log exposure" (Rel. log E). The use of a relative instead of an absolute scale of exposures does not affect the shape of the H and D curve in any way but is means that absolute speed values cannot be determined from the curve. In practice, a negative usually occupies part of the toe of the curve as well as part of the straight line. Then gamma alone gives an incomplete picture of the contrast of an emulsion. A more useful measure of contrast is given by the contrast index which takes into account the toe of characteristic curve. Although, in this text gamma and contrast index are used synonymously, it is appreciated that a difference in absolute values exist. The nonlinearities introduced in recording information in the toe of the H and D curve, especially in the contact printing stage (Fig. 5.1.4) is a condition which has to be tolerated in order to suppress the 'd.c.' background. The large portion of the straight-line part of the H and D curve for Ilford ortho (SP348) enables the coded picture to be easily accommodated within its range.

5.1.6. Calibration of the Characteristic Curve

The films were calibrated using the Kodak step tablet No. 2 (CAT 152 3106) and a Joyce Lobel Microdensitometer. The step tablet was placed in contact with the film under test and exposed from a uniform diffuse source. The temperature of the water bath and hence developer was maintained at a constant 20°C. The films were developed within a range of the recommended development time of the manufacturer and then rinsed, fixed, washed and allowed to dry.

The developed negatives were placed in the microdensitometer and the densities of the steps recorded. These measured density values are then plotted against the calibrated density values of the Kodak step tablet. This gives the characteristic curve for the film under the development conditions. The slope of this curve will give the gamma of the film.

5.2 MATHEMATICAL TREATMENT

If the coded picture is recorded in the straight line position of the H and D curve

$$D = -\log T_i \qquad (5.2.1)$$

where D is the density.

T_i is the intensity transmittance of the developed film.

D may also be written as

$$D = \gamma \log E - D_o \qquad (5.2.2)$$

where γ is the slope of linear region of the H and D curve

D_o is the intercept on D axis (Fig. 5.1.2) after extending linear region to cut D axis as if there were no toe.

From Eqns (5.2.1) and (5.2.2) we get

$$\log T_i = -\gamma \log E + D_o \qquad (5.2.3)$$

If the first stage viz., coded picture formation gives, as it does, a negative transparency, then let us use the subscript n to denote this. Re-writing Eqn (5.2.3) we get

$$\log T_{in} = -\gamma_n \log E + D_o \qquad (5.2.4)$$

Now from Eqn. (5.1.5)

$$E = It$$

So, Eqn. (5.2.4) becomes

$$\log T_{in} = -\gamma_n \log (It) + D_o \qquad (5.2.5)$$

where I is the incident irradiance for coded picture formation.

Eqn. (5.2.5) can be expressed as

$$T_{in} = K_n I^{-\gamma_n} \qquad (5.2.6)$$

where $K_n = 10^{D_o}.t^{-\gamma_n}$ and is a positive constant.

Eqn. (5.2.6) demonstrates that the intensity transmittance T_{in} of the coded picture is nonlinear with respect to the incident irradiance I of the object.

If we use this coded picture(with the clear region surrounding the convolution area blacked out) to correlate with the original code we observe a contrast-reversed reconstruction on the image plane. That is a negative image (black) on a positive (white) background. Due to the nonlinear recording process and the subsequent contrast inversion at the image plane, the 'd.c.' background cannot be clipped by the photographic process.

However, contact printing of the coded picture gives a positive power law between T_{in} and I. Thus the image appears as a positive on a 'd.c.' background and photographic clipping techniques can be applied to reduce its effect.

Let the intensity transmittance of the contact print be, T_{ic} and

$$T_{ic} = K_c \, I_c^{-\gamma_c} \tag{5.2.7}$$

where K_c is a positive constant and equal to $10^{D_o}.t^{-\gamma_c}$

I_c is the incident irradiance on the coded picture and subscript c denotes contact printing.

Now,the intensity transmittance of the coded picture formation stage T_{in} given by Eqn. (5.2.6) is.

$$T_{in} = K_n \, I^{-\gamma_n}$$

Now,

$$I_c = I_p \times T_{in} \tag{5.2.8}$$

where I_p is the illuminating irradiance during contact printing.

From Eqns. (5.2.7) and (5.2.8) we get;

$$T_{ic} = K_c (I_p T_{in})^{-\gamma_c}$$

Using Eqn. (5.2.6) we get

$$T_{ic} = K_c (I_p K_n I^{-\gamma_n})^{-\gamma_c}$$

$$T_{ic} = (K_c K_n^{-\gamma_c} I_p^{-\gamma_c}) I^{\gamma_n \gamma_c}$$

$$T_{ic} = K I^{\gamma_n \gamma_c} \tag{5.2.9}$$

where $K = K_c K_n^{-\gamma_c} I_p^{-\gamma_c}$ is a positive constant.

We have a linear relationship between the intensity transmittance T_{ic} of the contact print of the coded picture and the incident recording irradiance I of the object if

$$\gamma_n \gamma_c = 1 \tag{5.2.10}$$

Then

$$T_{ic} = KI \tag{5.2.11}$$

If $\gamma_n \gamma_c > 1$ then we have a nonlinear positive power law but with a possibility of suppressing the 'd.c.' background by photographic clipping.

5.3 GRAPHICAL TREATMENT

Let us now consider the process of coded picture formation and contact printing in relation to the H and D curve (Fig. 5.3.1).

If we use a low contrast index film, with a large logE range for the coded picture formation, we then ensure that the intensity range of the object can be recorded on the linear part of the H and D curve. Thus we map this intensity range linearly onto a density range. During the contact printing stage we must ensure that this density range can be accommodated within the linear range of the H and D curve of the film used for contact printing. Thus we translate this density range (which has become an "intensity range" as far as the contact printing is concerned) into a further density range. It is evident that providing clipping does not occur (i.e. information lost at shoulder and toe of H and D curve) we have the density range of the coded picture reproduced in a positive form.

By judicious variation of exposure, the contact printing stage can be recorded on the linear part of the H and D curve occupying a broader density range. This enables the intensity range of the object to be mapped into a "contrasty" density range as opposed to the "soft" density range in the coded picture. It is necessary of course to have a "contrasty" contact print to ensure that

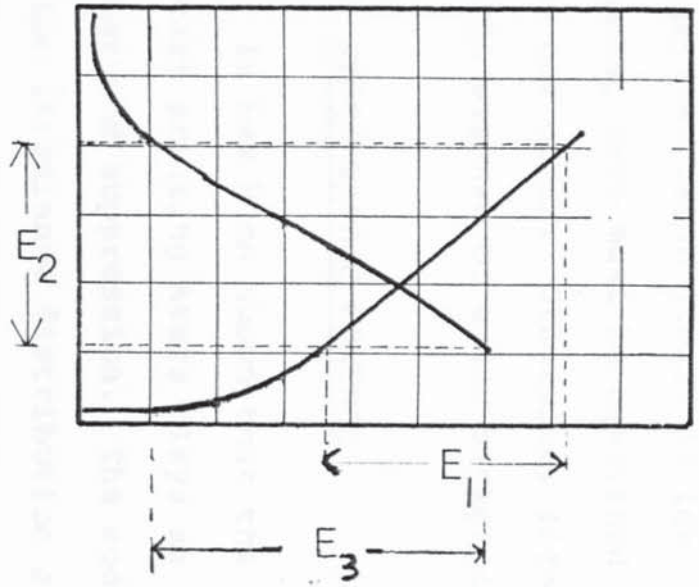

Fig.5.3.1 Effects of linear range on coding and contact printing.

E_1 = subject brightness range for coded picture

E_2 = resulting negative range for coded picture

also E_2 = effective subject brightness range for contact print

E_3 = resulting density range of contact print

part of the "d.c." background can be suppressed. This is achieved by making the reconstructions on medium contrast index films. We know that from Eqns (5.2.10) and (5.2.11) that when $\gamma_n\gamma_c=1$, $T_{ic}=KI$. Consider what happens when $\gamma_n\gamma_c>1$. In practice, it is desirable to keep $\gamma_n<1$ and make $\gamma_c>1$ thus enabling their product to be unity and get a "contrasty" contact print. We can readily make $\gamma_n\gamma_c>1$ for "dilute" objects where the brightness range (logE) is low but with continuous tone objects, care must be exercised to ensure that clipping does not occur. Otherwise, information is sacrificed at the expense of a low background (Fig. 6.2.1).

5.4 PHOTOGRAPHIC CONTROL

It has been shown that the contrast index of the contact printing stage plays an important role in "d.c." background suppression. The coded picture is a convolution of the irradiance distribution of the object with the intensity PSF of the coded aperture. Thus we would expect the density range of the coded picture to be a function of the coded aperture.

The $\frac{1}{r}$ intensity variation of the shoulder of the Annulus and Twin Annulus PSFs imposes a restriction to γ_c, the contrast index of the contact print. This is due to the large density range recorded on the coded picture. On the other hand the intensity PSFs of the FZP and URA

necessitates the use of a high γ_c.

The contact printing stage essentially forms the first stage in the "d.c." background suppression. A "contrasty" contact print will reduce the transmission of the unwanted cross-correlation terms which form the "d.c." background.

When recording the reconstructed image we can clip this, already reduced, background further, by using a medium or high γ film. This process forms the second and final stage in "d.c." background suppression. This latter stage can be illustrated by considering the reconstruction shown schematically of a point source object with the Annulus as the coded aperture (Fig. 5.4.1.). The figure shows the reconstruction (as it would look) if formed on a low contrast index film. By recording the reconstruction on a high contrast index film (again shown schematically) on Fig. 5.4.2 we can see the effect of "d.c." background suppression. This is readily achieved by using the clipping nature of high γ films. Barrett et al.[18, 46] propose a rho-filter to remove $\frac{1}{r}$ effect of the shoulder in the Annulus PSF, here a simple photographic technique is proposed. Our technique only applies of course to point source and dilute objects.

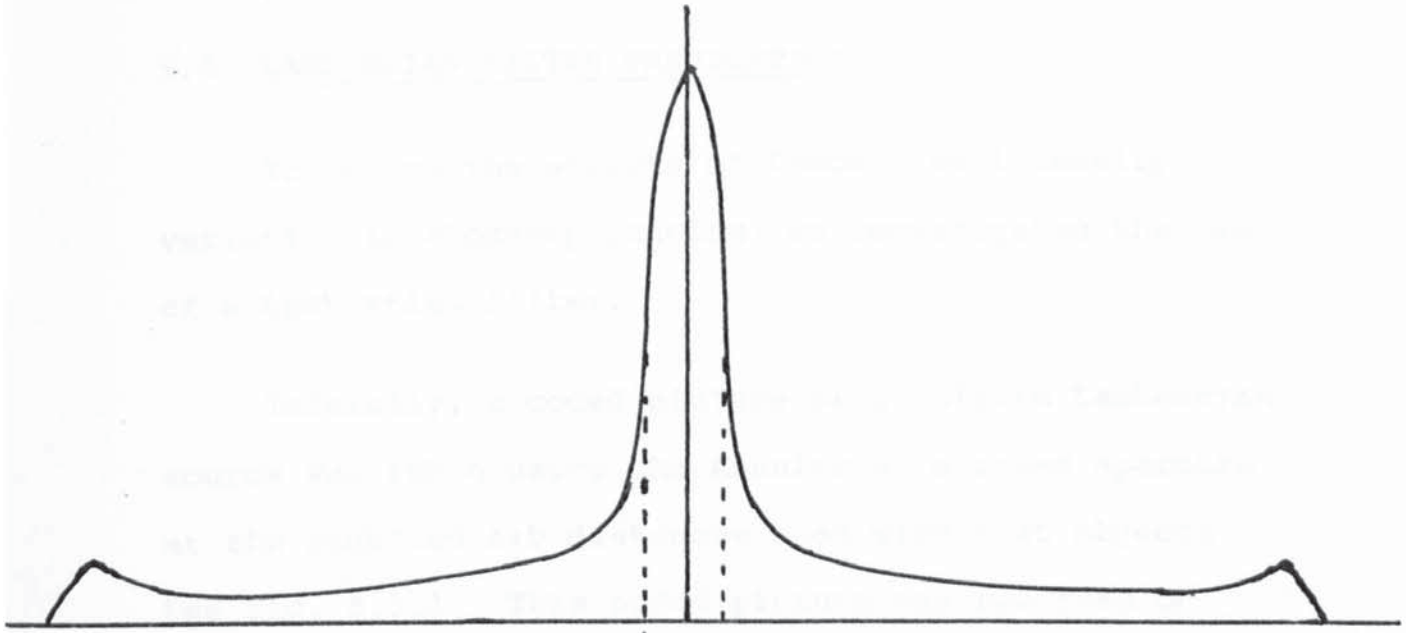

Fig.5.4.1 Sectional view of a reconstruction of a point source object on a low gamma film.

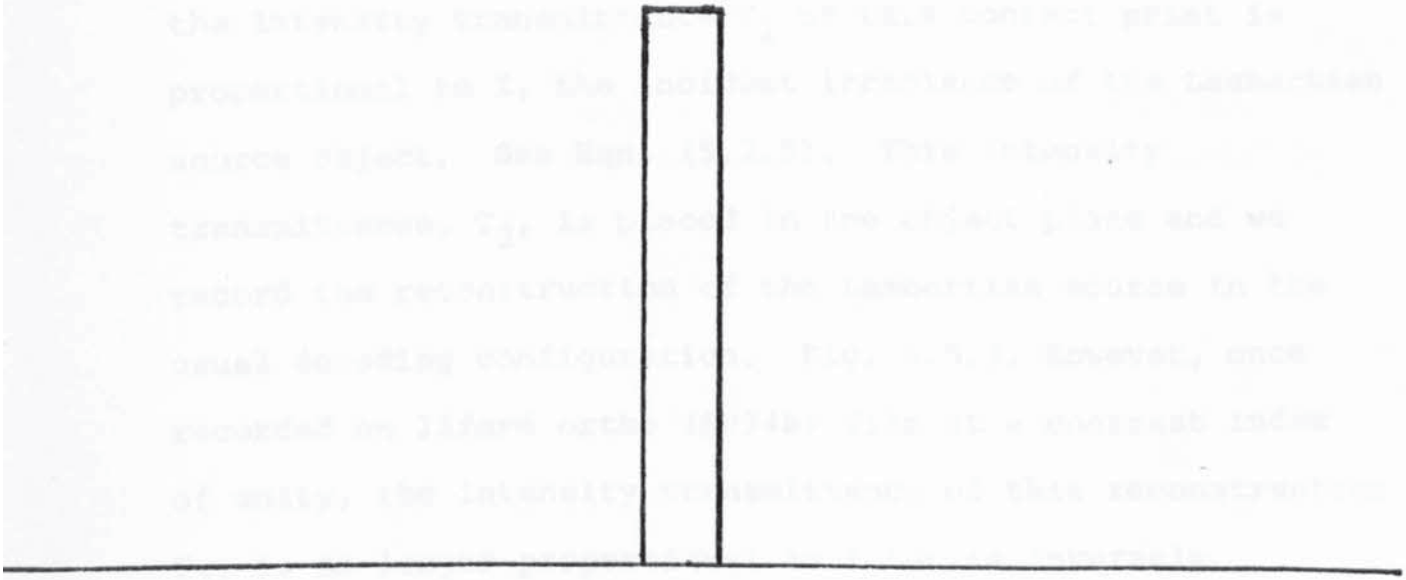

Fig 5.4.2 Sectional view of a reconstruction of a point source object on a high gamma film.

5.5 LAMBERTIAN FILTER FABRICATION

To reduce the effects of Lambertian intensity variation in close-up imaging, we investigated the use of a Lambertian filter.

Initially, a coded picture of a uniform Lambertian source was taken using the Annulus as a coded aperture at the required a:b distances used with test objects. See Fig. 5.5.1. This coded picture was recorded on Ilford ortho (SP348) and developed in Ilford PQ diluted (1+9) at 20°C for 3 mins to give a contrast index of 1.0 (unity). The intensity transmittance of this coded picture T_1 is inversely proportional to I.

A contact print of this coded picture was formed under identical processing conditions. Fig. 5.5.2. Thus the intensity transmittance T_2 of this contact print is proportional to I, the incident irradiance of the Lambertian source object. See Eqn. (5.2.9). This intensity transmittance, T_2, is placed in the object plane and we record the reconstruction of the Lambertian source in the usual decoding configuration. Fig. 5.5.3. However, once recorded on Ilford ortho (SP348) film at a contrast index of unity, the intensity transmittance of this reconstruction T_3, is no longer proportional to I but is inversely proportional to I. This reconstruction T_3 is termed the Lambertian Filter and it encompasses the $\cos^8\theta$ intensity

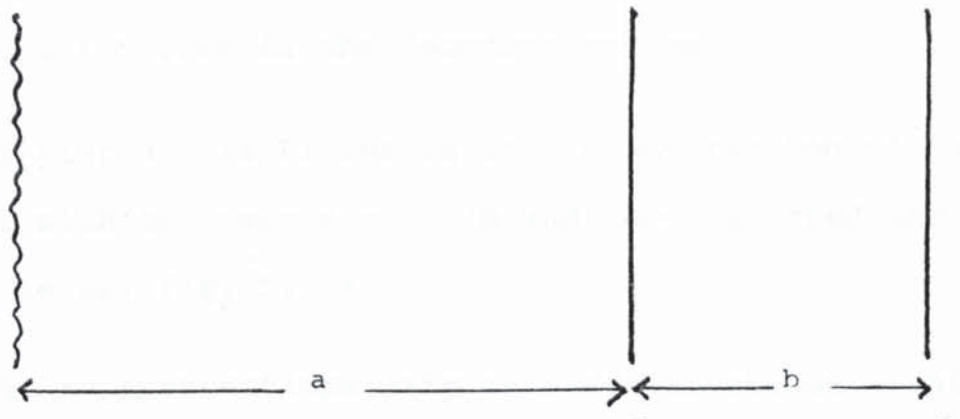

$T_{coded\ picture} \propto I^{-\gamma_1}$

$T_1 \propto I^{-1}$ (see text)

Fig.5.5.1 First stage of Lambertian Filter fabrication.

S- diffuse Lambertian source, C- coded aperture,
G- photographic film, a- source to coded aperture distance,
b- coded aperture to coded picture distance.

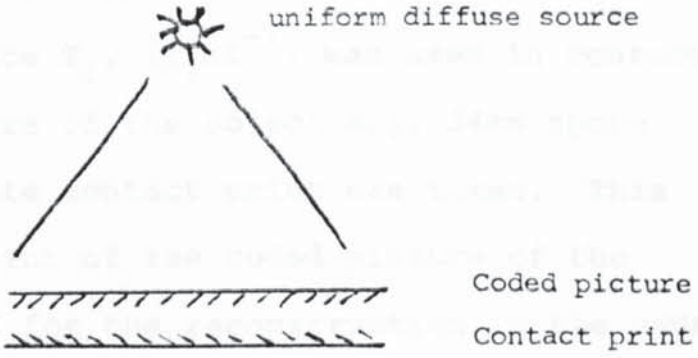

$T_{contact\ print} \propto I^{-\gamma_1 \gamma_2}$

$\gamma_2 = 1$ (see text)

$T_2 \propto I$

Fig.5.5.2 Second stage: Contact Printing

variation inherent in the decoding system.

We placed this Filter in the reconstruction plane in contact with the recording film and reconstructed the test objects, Fig. 5.5.4.

The reconstructions with this Filter showed a uniform background over the entire film plane. However, the intensity variation in the reconstructed image still persisted and it was this variation which appeared on the uniform "d.c." background provided by the Filter.

Instead of trying to overcome the $\cos^8\theta$ variation as described above, we attempted to overcome a $\cos^4\theta$ variation. The initial coded picture stage of the uniform diffuse source T_1, $(T_1 \alpha I^{-1})$ was used in contact with the coded picture of the object e.g. 34mm spoke target and a composite contact print was taken. This composite contact print of the coded picture of the object was then used for the reconstruction in the usual manner. Once more the intensity variation in the reconstructed image persisted.

We concluded that this intensity variation was due to the intensity variation of the SPSF of this coded aperture and that Lambertian effects were insignificant in our coding and decoding configuration.

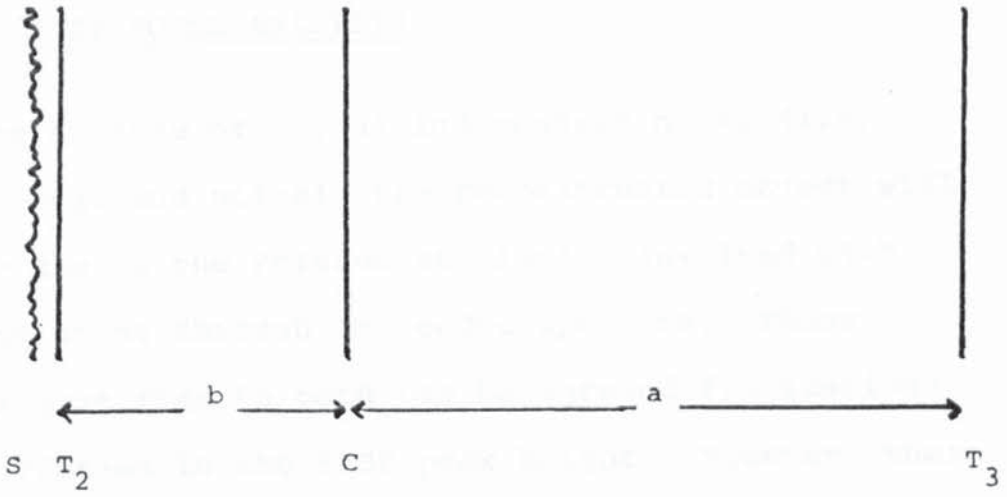

$$T_3 = I^{-\gamma_3}$$

$$\gamma_3 = 1 \text{ (see text)}$$

$$T_3 = I^{-1}$$

Fig. 5.5.3 Third stage: Final Filter fabrication.

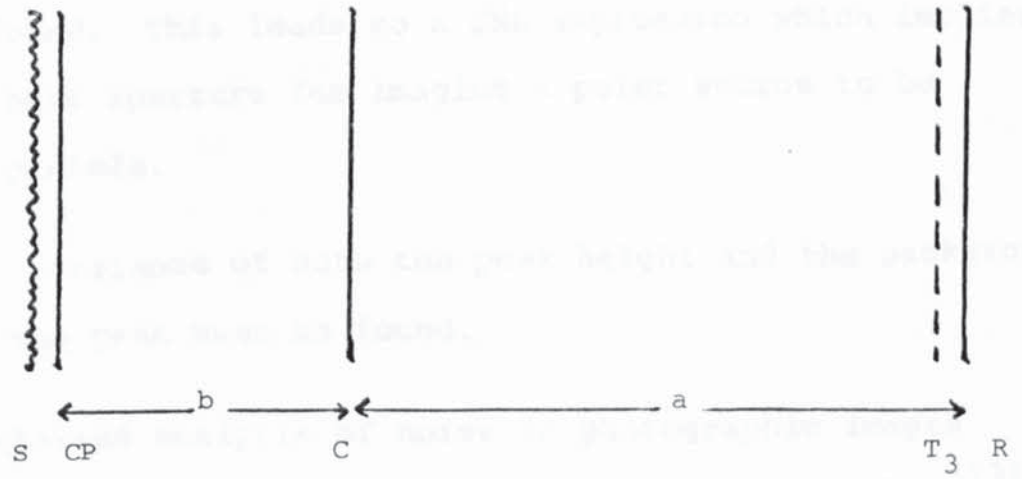

Fig.5.5.4 Using the Lambertian Filter.

CP- coded picture of object
T_3- Lambertian Filter
R - recording plane for reconstruction

5.6 ELEMENTARY NOISE ANALYSIS

In the absence of signal independent noise (i.e. detector background noise) the reconstructed object will have noise due to the Poisson statistics involved with the photons going through the coded aperture. These statistics give rise to both the background fluctuations and the variation in the SPSF peak height. However, there are several ways to define this noise term.

(1) Variance of the fluctuation of the peak height. This is an applicable noise term if one is interested solely in the intensity of a point source. It leads to a SNR expression which predicts the best aperture to be one that is completely open, i.e. one big hole.

(2) Variance of the background in which the peak must be found. This leads to a SNR expression which implies that the best aperture for imaging a point source to be a single pinhole.

(3) Variance of both the peak height and the background in which the peak must be found.

A detailed analysis of noise in photographic images is found in "Image Science" by J. C. Dainty and R. Shaw[73]. Here, we briefly describe the parameters affecting the SNR of a photographic image in terms of the Detective Quantum Efficiency (DQE).

DQE is defined as

$$DQE = \left\{\frac{(S/N)_{OUT}}{(S/N)'_{OUT}}\right\}^2 \times 100 \text{ per cent} \qquad (5.6.1)$$

where $(S/N)_{OUT}$ is the signal-to-noise ratio of the output from the image recording process under consideration and $(S/N)'_{OUT}$ denotes the output signal-to-noise ratio of a hypothetical "ideal" image recording system registering every single exposure photon.

In practice it is found that at an exposure level E,

$$DQE_E = \frac{(\log_{10}e)^2\gamma_E^2}{E.G_E} \times 100 \text{ per cent} \qquad (5.6.2)$$

where γ_E is the slope of the characteristic curve at the exposure level E photons μm^{-2}.

G_E is a measure of the granularity at this point. Granularity, G, is defined as the objective measure of the inhomogeneity of the photographic image and is determined from the spatial variation of density recorded with a microdensitometer. $G = \sigma\sqrt{2A}$ for materials exposed to light. This is Selwyn's Law, where σ = standard deviation of the density deviations, and A = aperture area of micro-densitometer.

Eqn (5.5.1) can also be expressed as

$$DQE \propto \frac{(\text{Contrast})^2 \times \text{Speed}}{\text{Granularity}}$$

which implies

$$(S/N)_{OUT} \propto \text{contrast } (\gamma_E)$$

Let us consider the effect of DQE transfer for a two-stage process as in the case of contact printing. Let the DQE of the first stage (coded picture formation) be

$$DQE_1 = \varepsilon_1(q) = \frac{(\log_{10}e)^2 \gamma_1^2(q)}{E_q G_1(q)} \tag{5.6.3}$$

at the absolute exposure level, E_q, quanta per unit area.

Now suppose the exposure level E_q of the first stage correspond to a density D in the final print image of the second stage (viz, contact print). The magnitude of the overall gamma of the two stages will be

$$\gamma(q) = \gamma_1(q)\ \gamma_2(D) \tag{5.6.4}$$

The overall noise G(q) can be obtained by assuming that noise of the first stage is transferred through the characteristic curve of the second stage and then adds to that of the second stage at density D.

$$G(q) = \gamma_2^2(D) G_1(q) + G_2(D) \tag{5.6.5}$$

Substituting for γ_1 and G_1 in Eqn. (5.5.3) we get for the overall DQE $\varepsilon(q)$

$$\varepsilon(q) = \frac{\varepsilon_1(q)}{\{1 + \dfrac{G_2(D)}{G_1(q)\gamma_2^2(D)}\}} \tag{5.6.6}$$

when

$$\frac{G_1(q)}{G_2(D)}\,\gamma_2^2(D) >> 1 \qquad (5.6.7)$$

the overall DQE, $\varepsilon(q)$, will be that of the first stage with a negligible reduction due to the second stage.

The justification of defining the overall DQE, $\varepsilon(q)$, in terms only of the exposure level, E_q, relating to the original exposure of the first stage, is that it is at this first camera stage where all available exposure light should be used efficiently; so DQE is measured with respect to this amount of light.

The amount of light available for the second, contact printing stage, is usually at our disposal and of negligible interest from a DQE criterion. This is why the characteristics of the contact printing stage have been specified as functions of image density level.

Thus the basic requirement of the first (camera) stage is not those of camera speed but of maximum DQE.

CHAPTER 6

CODED APERTURE IMAGING - OPTICAL SIMULATIONS

CHAPTER 6

CODED APERTURE IMAGING - OPTICAL SIMULATIONS

6.1 EXPERIMENTAL PARAMETERS

The objects were constructed as transparencies on photographic film. The 'square' object and spoke targets were formed on Kodalith Ortho type 3 (2556) film. The continuous-tone thyroid phantom was formed on Ilford Technical Orthochromatic (SP348) film. The shape of the square object was determined by a sequence of random numbers such that even numbers in this sequence gave rise to clear squares and odd to opaque squares. It consisted of 64 unit cells out of which approximately 50% were clear and hence transmitting, from an overall field of 361 mm^2. Both spoke targets were transmitting through 50% of their respective fields. Spoke target A occupied an area of 227 mm^2 and spoke target B, an area of 908 mm^2. The thyroid phantom was constructed by superimposing several layers of neutral density filters until a negative was produced which had an intensity range of 12:1 between the "hottest" and "cold" spot.

The object to code distance 'a' varied from 55mm to 75mm and the code to coded picture distance 'b' from 25mm to 45mm. In particular, the distances a:b varied as follows:- 75:25::55:45.

A wooden box was constructed with accurately machined slits to hold the film cassettes in planes which were

ANNULUS	TWIN ANNULUS	FRESNEL ZONE PLATE	UNIFORMLY REDUNDANT ARRAY
D_1=2o mm w =O.13mm a= 75mm b= 25mm	D_1=2Omm D_2= 4O mm w_1=O.13 mm w_2=O.21mm a=75mm b=25mm	D =5Omm w_{min}= O.11mm a=75mm b=25mm	r= 73,s=71 w_{min}= O.3mm a=15Omm b=1OOmm

Fig.6.1.1 Details of the Coded apertures used in the optical simulations.

D- diameter of the coded aperture,w- the width of the smallest aperture of Code,
a- object to coded aperture distance, b- coded aperture to coded picture distance.

parallel to each other. The object transparencies were placed in contact with a uniform diffuse source.

Fig. 6.1.1 shows dimensional details of the various coded apertures used.

6.2 FRESNEL ZONE PLATE

The FZP is unique amongst coded apertures in that the coded picture thus formed can be decoded by Diffraction, Deconvolution and Correlation. The original Mertz and Young noncoherent holograms were decoded by diffraction. A reduced size transparency of the noncoherent hologram was made such that the individual FZPs of the ensemble had convenient focal lengths, and this reduced transparency illuminated with coherent light. The focusing action of the FZPs reconstructed the star field.

A FZP has both positive and negative focal lengths so that energy is spread outwards as well as being focused. Thus every point has a flare spot (halo) around it. The removal of these extra haloes has been discussed by Bragg and Rogers[74].

The major problems with optical reconstruction techniques is the removal of the d.c. bias (undiffracted light) which passes through the hologram to raise the background level.

To avoid the problems of d.c. bias and haloes which

are in fact secondary holograms, several authors have used off-axis zone plates analogous to the off-axis holography of Leith and Upatnieks. This device has the effect of throwing the beam a known distance to one side as well as focusing it. The unwanted negative power in the zone plate is now associated with a deviation in the opposite direction, so that the unwanted blur halo clears the wanted reconstruction. This particular technique works very well with an assembly of point sources, since each point source is equivalent to a wide range of spatial frequencies. These frequencies interact with the zone plate to give a sharp shadow. Otherwise, the off-axis zone plate acts rather like a spatial frequency filter and only parts of the shadow are sharp (Leifer et al.[75]) and then only if the appropriate frequencies are present in the object. An off-axis zone plate has a limited range of frequencies; in particular it has a low frequency cut-off. If the object has no frequencies in the pass band of the zone plate then it has to be modulated with a grating in the manner of Barrett et al.[8]. This modulation reduces the intensity of the recording but most worthwhile results have been obtained with continuous tone objects.

Silva and Rogers[19] have adopted the noncoherent correlator to decode the noncoherent holograms (coded pictures) in noncoherent light. A technique was developed to reduce considerably the d.c. bias which forms a major drawback in noncoherent optical processing.

Again, worthwhile results were obtained with dilute objects. The SPSF of an amplitude FZP has its central maximum surrounded by a dark ring. This is in contrast to the SPSF of a complex-amplitude and phase FZP, which has a uniform shoulder surrounding the central peak. The origins of this dark ring lies in the restriction to positive-only functions in noncoherent optical processing and to the finite extent of the FZPs used. So this dark ring presents an artifact in FZP imaging when the reconstructions are performed in noncoherent optics. For dilute objects, this dark ring produces a desirable edge enhancement effect but with continuous tone objects this artifact will be detrimental.

Silva and Rogers[19] have also used an off-axis FZP as a coded aperture and decoded the resulting coded picture in noncoherent light. The object was modulated by a grating in the manner of Barrett et al.[8] so that its frequencies were projected onto the pass band of the off-axis FZP. The reconstructions were marred by a set of fringes superimposed on the image. These fringes are a characteristic of the SPSF of the off-axis FZP under noncoherent optical processing and is evidenced by the limited range of frequencies, in particular the low frequency cut-off, in an off-axis FZP. These artifacts can be removed by low pass filtering without loss of resolving power.

The reconstructions presented in this thesis are

performed in a lensless noncoherent correlator. The coded picture, subject to suitable processing, is correlated with the original code - the projective magnifications being performed automatically in the coding process due to its geometry and rectilinear propagation of light.

The conditions of determining spatial resolution and minimising Lambertian intensity variation described in Section (3.3) of Chapter 3 are applicable here too. The coded pictures were formed on Ilford ortho (SP348) film and processed to give a contrast index (gamma) of unity. The coded picture was recorded on the linear range of the H-D curve. If we make the contact print under the same processing conditions viz. $\gamma=1$, then, the reconstructed image is found to be totally immersed in 'd.c.' light or the background. We have developed a technique to reduce considerably the effect of the 'd.c.' light background. Now, if we make the contact print on a high γ film such as Kodalith ortho type 3 (2556) film, we can convert or map the density range of the coded picture over a larger density range by suitable switching, providing too much information is not clipped at the shoulder and toe of the H-D curve. In practice, the degree of clipping which occurred in the contact prints of the coded pictures for the various objects, have been of an acceptable nature. Now, if we use this high γ contact print to correlate with the original code in the decoding procedure and also use a

medium γ film such as Ilford line to reconstruct, thus clipping the shoulder of the PSF, we can improve the contrast greatly.

Consider the coded picture formation form the holographic viewpoint. Each point in the object is considered to generate its own FZP pattern on the coding plane, whose amplitude and phase is determined by the intensity and position respectively of the FZP pattern. Here, in the noncoherent case, the phase of the FZP pattern is fixed by the code as we have shadow casting and only encode the amplitude information of the object in terms of intensity. So the high γ contact print essentially does what was described in the previous paragraph.

A glance at the autocorrelation of the FZP (Fig. 6.6.1) reveals an inherent artifact introduced in noncoherent correlation decoding. This is, of course, as a result of the restriction to binary functions in noncoherent light and to the finite size of the FZPs used. The central bright spot is seen surrounded by a dark ring and the whole looks very similar to the Airy pattern[76-78]. A point source object when reconstructed would appear as the autocorrelation of the FZP code. This dark band surrounding the central maximum causes a 'ringing' effect at the edge of the object as seen from the reconstruction of a disc object. (Fig. 6.2.1). This ringing effect is noticeable in the reconstructions of the thyroid phantom and the square object. These reconstructions were formed on Ilford line film and

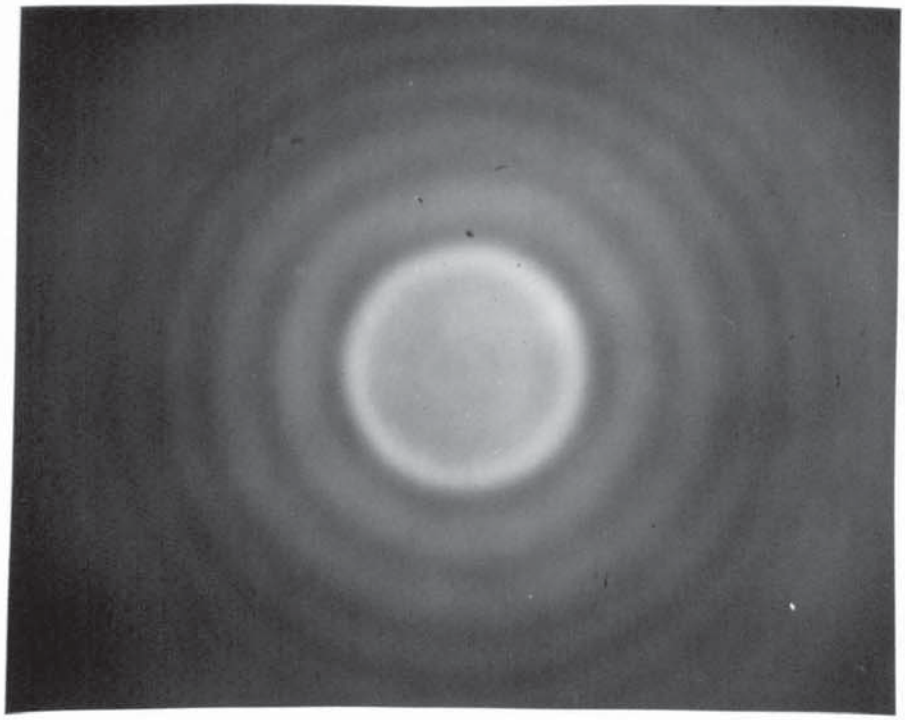

Fig.6.2.1 Reconstruction of a disc object showing the ringing effect discussed in text.

developed in Phenisol diluted (1+4). The reconstruction of the spoke target shows the spatial resolution capable from this aperture (see Eqn. 3.3.9) under the coding conditions used. It was formed on Kodalith ortho type 3 (2556) film.

6.3 ANNULUS

The use of an Annulus as a coded aperture has been widely reported. Coded pictures obtained from this code have been decoded electronically[44], digitally[46] and by coherent optical means[45,47-49]. We, of course, will limit ourselves to a noncoherent optical approach.

Conditions for optimum coding and decoding are found in Section (3.3) of Chapter 3. Additionally, a restriction to the object diameter imposed by the nature of the autocorrelation function of the coded aperture is obtained thus. The autocorrelation of the Annulus has a central peak surrounded by a secondary peak (Fig. 6.6.1) at a radial distance x given by

$$x = \tfrac{1}{2}D\left(\frac{a+b}{b}\right) \qquad (6.3.1)$$

where D is the mean diameter of the Annulus. To avoid the reconstruction from being marred by this secondary peak, Eqn.(6.1),the object diameter must be less than 2x.

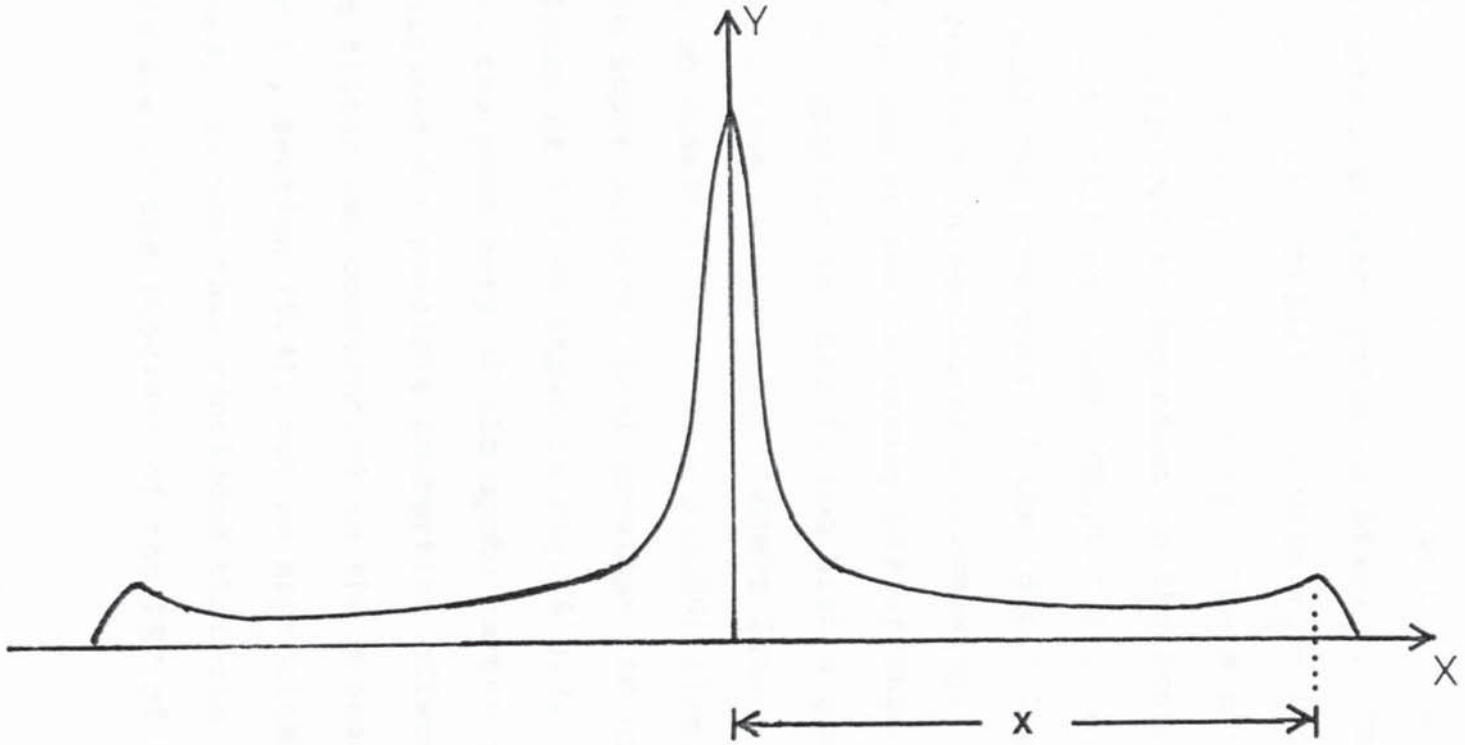

Fig.6.3.1 Sectional view of the autocorrelation of an Annulus.

In the optical simulation we coded our objects (Stage I) onto a low contrast index (gamma) film - Ilford ortho (SP348) film with γ_1=0.7. Exposures were controlled so that the linear region of the H-D curve of the film was used. In order to decode the coded pictures we need to make a contact print of Stage I. This is also made on Ilford ortho (SP348) film with γ_2 = 1.5, thus keeping the overall $\gamma = \gamma_1\gamma_2 \sim$ unity. The suppression of the 'd.c.' background is dependent on the contrast index of this contact printing stage (Chapter 5). A high γ at this stage will cut down most of the 'd.c.' light which is the major drawback in noncoherent processing. However, due to the nature of the intensity PSF of this coded aperture, information is lost if too high a gamma is used. The reconstruction of the square object from a contact print made on Kodalith ortho type 3(2556) film, developed in Kodalith Super diluted (1+3) developer to give a contrast index of 3.8 as shown in Fig. 6.3.2. The intensity fall-off at the periphery of the spoke target reconstructions was investigated for possible Lambertian effects. A Lambertian filter was constructed in the manner described in Chapter 5 , section (5.4), but no appreciable improvement was obtained. It was thus concluded that the intensity fall-off is due to the shoulder of the PSF of the coded aperture.

It has been mentioned in Chapter 3 that resolution was a function of a, b, w and λ. We have used the Annulus

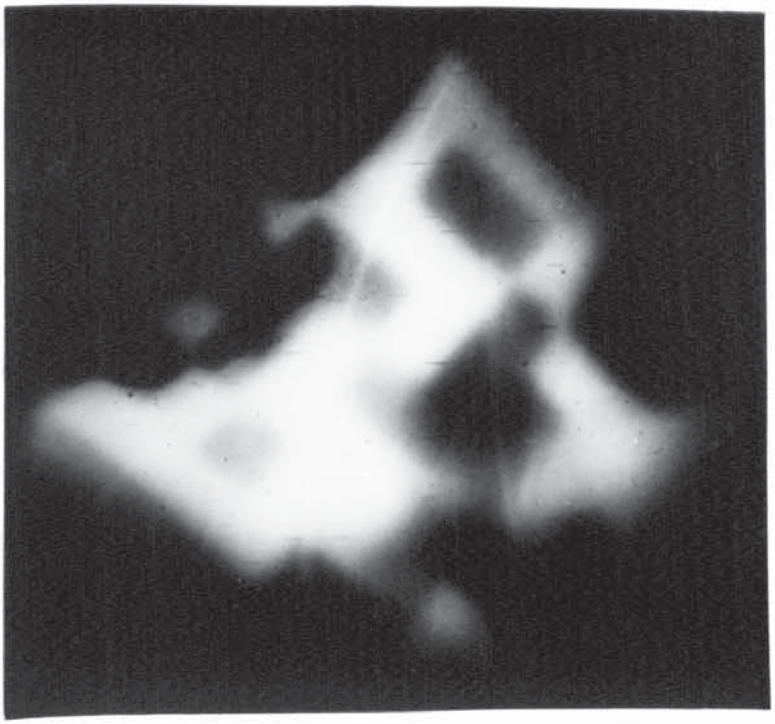

Fig.6.3.2 Reconstruction of the square object when clipping has occured in the contact printing stage.

to investigate these relationships. By varying w and keeping the other parameters constant we can show the effect of w as it increases from the diffraction limit. Fig. 6.3.3 shows the reconstruction of the square object with w = 0.5mm and Fig. 6.3.4 with w = 0.14mm. The blurred edges are due to the lack of high frequencies and this becomes evident from the increased diameter of the autocorrelation function. A similar effect can be shown by keeping w and λ fixed whilst varying a and b.

6.4 TWIN ANNULUS

The use of a Twin Annulus as a coded aperture has been presented by Silva and Rogers.[50]. In appearance it can be thought of as an aperture which lies between the Annulus and the FZP. In practice, it offers an improvement in the photon count rate available at the detector when compared with the Annulus, the shoulders of the SPSFs of the two coded apertures having a very similar nature. Although in terms of aperture transmission the FZP has an advantage over the Twin Annulus, in terms of photon counts, our processing technique gives us a better image contrast for images from the Twin Annulus when compared with both Annulus and FZP images (Fig. 6.6.1).

Conditions for optimum coding and decoding are found in Section 3.3 of Chapter 3. The restriction imposed on the object diameter by the nature of the autocorrelation function is dependent on the radii of the two annuli in the coded

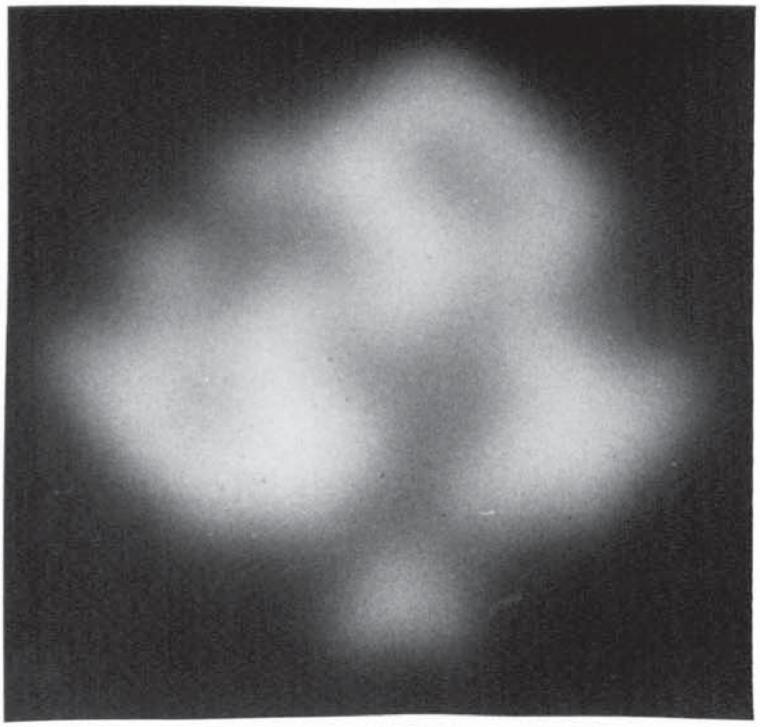

Fig.6.3.3 Reconstruction of the square object with w=0.5mm showing effect of increased w on resolution.

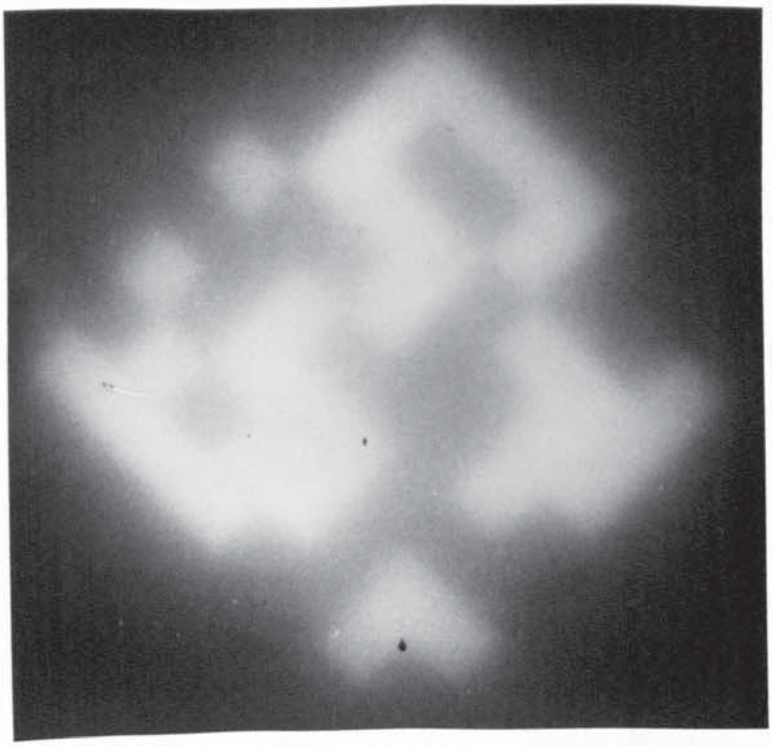

Fig.6.3.4 Reconstruction of the square object with w=0.14mm under identical coding conditions to Fig.6.3.3.

aperture. In general, the central peak is surrounded by several secondary peaks (Fig. 6.4.1). However, to avoid the reconstruction from being marred by the first side lobe (secondary peak) the object diameter must be less than 2x where

$$x = \tfrac{1}{2}(R-r)\left(\frac{a+b}{b}\right) \qquad (6.4.1)$$

where R is the radius of the outer annulus, and

r is the radius of the inner annulus.

If the single Annulus coded aperture has a radius r, and the Twin Annulus has inner and outer radii r and 3r respectively, then the restriction imposed on the object diameter would be identical for both coded apertures, assuming an infinitely large detector and neglecting $\cos^3\theta$ effects.

However, in our optical simulations details found in Fig.6.1.1the ratio of inner to outer radii r:R is in the ratio 1:2. In these particular circumstances the object diameter which can be successfully decoded (without interference from the side lobes) for the Annulus becomes 2x and the Twin Annulus x, for identical coding distances. This limitation was enforced upon us by the prior construction of the wooden box in which the transparencies were held. Referring to Fig.6.1.1we notice that the width w of the outer radius R is larger than the width w of the inner radius r. This gives rise to the loss of spatial resolution in the Twin Annulus reconstructions. (see Chaper 3).

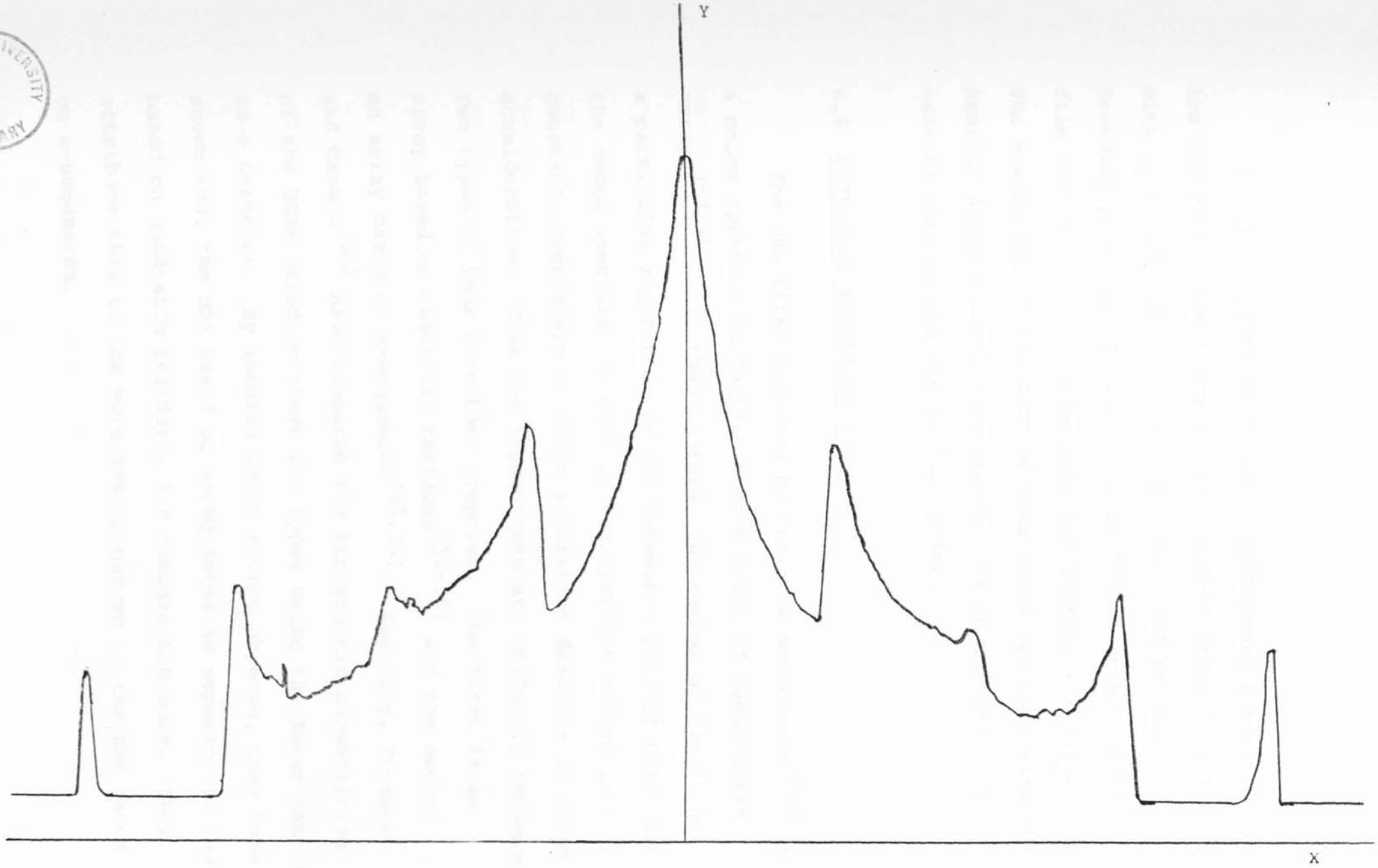

Fig.6.4.1 Cross-sectional view of the autocorrelation function of the Twin Annulus. R=2r.

The coded pictures of our objects were formed on a low contrast index (gamma) film - Ilford ortho (SP348)film with $\gamma_1 = 0.7$. The contact print required for the decoding process, was also made on Ilford ortho (SP348) film with $\gamma_2 = 1.5$ thus keeping the overall $\gamma = \gamma_1\gamma_2 \sim$ unity. The similarity of the SPSF of this coded aperture with the Annulus demands similar considerations to be taken into account when making the contact print.

6.5 UNIFORMLY REDUNDANT ARRAY

The URA first proposed by Fenimore and Cannon[52] as a coded aperture is derived from a class of pseudonoise arrays[57,59]. In these arrays, the number of times that a particular separation occurs between a pair of holes in the coded aperture (or ones in the aperture array) is a constant, regardless of which separation distance is under consideration. Thus the separations are uniformly redundant. Two types of URAs have been proposed. The first is an array based on quadratic residues[52-56] and the second an array based on m-sequences[55,59]. Recently, Fenimore and Cannon[55] have compared the tomographic capabilities of the URAs based on these two types using the Anger camera as a detector. By imaging point source objects, they have shown that the URA based on m-sequences is superior to that based on quadratic residues, for tomographic work. They attribute this to the more random nature of the URA based on m-sequences.

In our optical simulations with extended and continuous-tone objects we used the type of URA based on quadratic residues. This was generated on the picture processing peripheral (FR80) attached to the IBM 360 computer at Chilton, Oxfordshire.

Consistent with the Fenimore approach, we used a 2r×2s mosaic version of the URA with r=73 and s=71 for coding. Once more optimum coding conditions are found in Section 3.3 of Chapter 3. The cross-correlation of a mosaic URA (e.g. 2r×2s)with a single or basic URA pattern (r×s) yields ideally a mosaic of delta functions. In order that the reconstructed images do not overlap, the diameter of object, x, should be such that

$$x < (\frac{a+b}{b})rw \qquad (6.5.1)$$

where w is now the unit cell size of the URA aperture. Decoding was performed by correlating the code with a mr×ms version of the coded picture (m not an integer).

$$\text{where} \quad mr\times ms \simeq |\{(\frac{a+b}{b})A(p,q)\}+(\frac{b}{a})O(x,y)| \qquad (6.5.2)$$

The coded pictures were formed on a low contrast index (gamma) film , namely Ilford ortho (SP348) with $\gamma=1$. The contact prints were made on Kodalith ortho type 3 (2556) film. Due to the high γ used in the contact printing stage - necessary to suppress the d.c. background - and the $\cos^2\theta$ Lambertian intensity variation present in the coded picture which is ~10%, it is relatively easy to obtain

a mr×ms version of the URA pattern and indeed a respectable version of a 2(mr×ms) version.

On examination of the autocorrelation (PSF) of the 2r×2s URA or r×s URA and the cross-correlation of a 2r×2s URA with an r×s URA under noncoherent correlation (Fig. 6.6.1), the central maximum is seen accompanied by a cross shaped array of artifacts on a hatched background. We believe this to be due to the non-ideal nature of the cell size as a result (ultimately) of the PSF of the photographic lenses used to form the coded aperture (see Fig. 6.5.1). Three examples of the variety of cell sizes, departing from the ideal, are shown to illustrate the problem of manufacturing the coded aperture as a photographic transparency. The 'switching' nature of the high γ film used to form the coded aperture transparency (Kodalith ortho type 3 (2556) film) poses additional problems. If we manufacture a URA with an effective aperture occupying say 50% of the cell area as in Fig. 6.5.2, thus making it a self-supporting URA, then we find its autocorrelation (shown in Fig. 6.5.3) or indeed the cross-correlation between a 2r×2s URA with a r×s URA, emphasises this nature of the background.

Since the recovered image is the convolution of the object with this PSF, artifacts are inevitably introduced in the reconstruction as evidenced in the results of (Fig. 6.6.1). Fenimore uses a balanced digital correlation method for decoding by computer where an array with negative

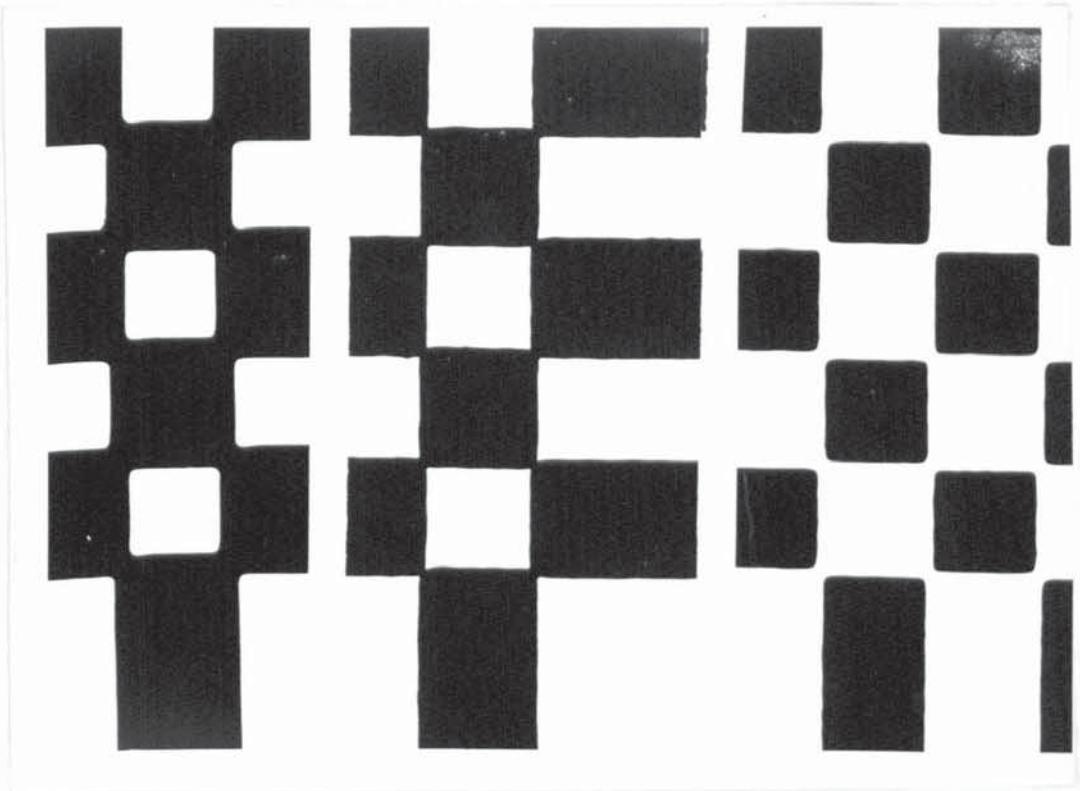

Fig. 6.5.1 Illustrates the problem of "rounding off" of the corners of a unit cell in the URA due to the PSF of the recording lens.

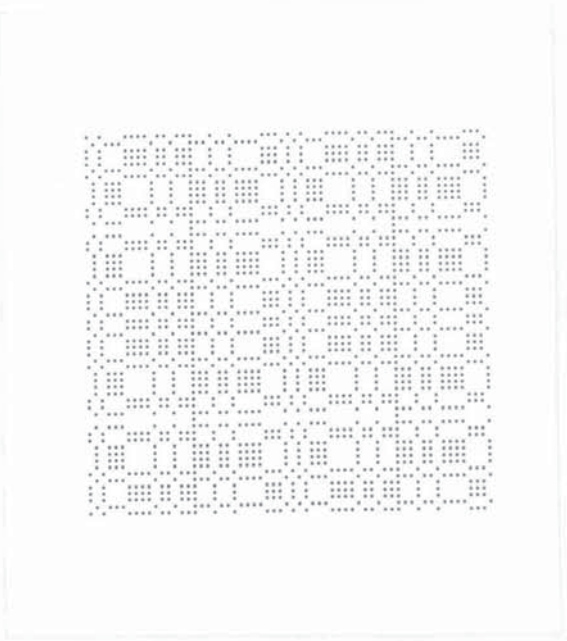

Fig. 6.5.2 A self-supporting URA with an effective aperture area occupying 50% of the cell area.

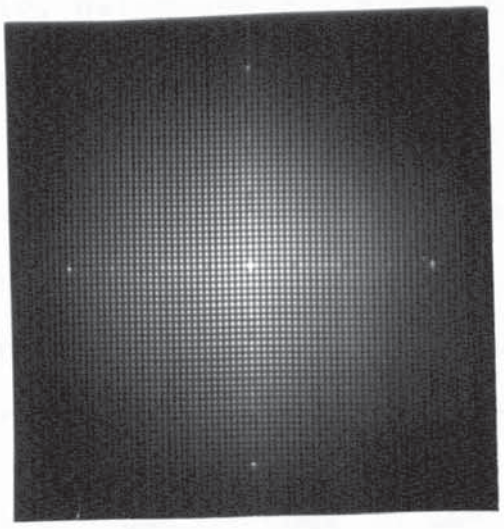

Fig. 6.5.3 The autocorrelation of the self-supporting URA emphasising the nature of the background.

transmittance values is used to correlate with the URA. The digital autocorrelation of a 2r×2s or r×s URA gives a central peak surrounded by a pyramidal shoulder. The digital cross-correlation of a 2r×2s URA with a r×s URA gives a central peak surrounded by a lattice of secondary peaks separated by $\frac{rc}{b}$ radians, interspaced by an uniform shoulder. By replacing the opaque cells (or 0's) of the decoding aperture by negative transmittance values (or -1's) and performing the digital cross-correlation, this uniform shoulder is reduced to zero, hence the term balanced correlation.

However, the latter operation cannot be performed with noncoherent optics without the introduction of a further 'd.c.' bias. Rogers[69] describes various means of mitigating this effect both directly (photographic control) and indirectly, using optical modulation techniques. We have restricted overselves to photographic control only. Also, the noncoherent optical cross-correlation of a 2r×2s URA with a r×s URA does not yield a central peak with an uniform shoulder for reasons outlined earlier. Thus for noncoherent optical decoding we have to contend with an undesirable PSF for the URA as a coded aperture.

As our decoding technique depends on the autocorrelation of the coded aperture or the cross-correlation between the coded aperture and a decoding aperture, being ideally a delta function and as we observe that the URA is noncentrosymmetric, the orientation of the coded picture

must be taken into account before reconstruction is attempted. (N.B. Coding is a convolution). Thus we rotate the coded picture by π radians (or if you prefer the code) in order to obtain the reconstruction. If, in fact, this rotation is not performed a contrast-reversed or negative image is formed on the detector plane. This is rather more difficult to record as the signal (negative) is embedded in the background and a rather noisy output is recorded. We can no longer use the clipping nature of films to suppress the background.

This contrast reversed image is due to the asymmetrical nature of the URA. The ability to use a mosaic version of the code and extract a central region to perform the decoding operation, a luxury not available with other coded apertures described earlier, led us to attempt to decode with a single coded picture - without the need for contact printing.

We formed our coded pictures directly onto a high γ film, namely Kodalith ortho type 3 (2556) film. Upon suitable processing with Kodalith super developer 2½ mins at 20°C the processed negative is masked by a mr×ms aperture. Again we have the choice of rotating either code or coded picture by π radians. Results of the reconstructions from the single coded picture and the contact printing stage are found in the last two columns of (Fig.6.6.1). The poor quality of the former reconstructions is evident from the nature of the autocorrelation of the URA under π-rotation. Here, the background appears dominant as it does in the

reconstructions. The Thyroid phantom and square object were reconstructed on Ilford line film whilst the spoke target was on Kodalith ortho type 3 (2556) film.

We also attempted as an exercise the single coded picture technique with the FZP. However, due to its circularly symmetric nature we could not implement contrast reversal and the resulting image showed very poor contrast.

6.6 RESULTS AND CONCLUSIONS

This section is basically a supplement to Fig. 6.6.1 in which all the results from the various coded apertures described in the previous sections are tabulated. The top row illustrates the type of coded aperture used and the first column shows the range of objects used. The autocorrelation functions (PSFs) of the various coded apertures, under noncoherent optical correlation, are found directly below the coded apertures on the second row. Directly below the specific coded aperture and beside the row containing the object lie the reconstructions.

Let us briefly summarise the results obtained by optical simulation of the coded apertures shown in Fig. 6.6.1, subject to a noncoherent optical decoding technique.

The Annulus and Twin Annulus reconstructions are characterised by their $\frac{1}{r}$ intensity fall-off in their PSFs. The loss of spatial resolution in the Twin Annulus

reconstructions is attributed to the increase in width w of the coded aperture. The reconstructions from the Twin Annulus show an improvement in contrast over the corresponding Annulus images. This is due to the increased energy in the central peak of the Twin Annulus PSF over that of the Annulus. The FZP reconstructions are characterised by the 'ringing' effect* described in section 6.2. Its effect on spatial resolution is shown up clearly in the spoke target reconstruction whilst its diagnostic effect is shown in the Thyroid phantom reconstruction. The undesirable background, characteristic of noncoherent optical correlation decoding from the URA PSF is evident in all the reconstructions. The conventional (contact printing) decoding results are presented in column 5 of Fig. 6.6.1, whilst the single coded picture reconstructions appear in the final column. The latter is evidenced by considerable loss of image contrast in comparison with the conventional case.

From the results of Fig. 6.6.1 which show the performances of the various coded apertures tested in this optical simulation, we conclude that the Twin Annulus and Annulus offer the best conditions for 'd.c.' background suppression in noncoherent optical correlation decoding.

* This "ringing" effect can be reduced by using an apodization filter with slight loss in spatial resolution.

FIG. 6.6.1 PERFORMANCE OF THE VARIOUS CODED APERTURES WHEN DECODING PLANAR OBJECTS USING A NONCOHERENT CORRELATION DECODING METHOD

Top Row : Aperture codes. L to R. Single Annulus, Twin Annulus, Zone Plate, URA I and URA II. The two URAs have the same basic structure but the second is inverted about the horizontal mid-axis to give a photographic negative of the first.

Second Row: Items 1-4 correlations of corresponding codes with themselves, Item 5 correlation of URA I with II giving a black dot in the centre.

Third Row : Extreme left. Input object of squares derived from a set of random numbers. Items 1-4 the reconstruction of this object using the codes at the top. Item 5. Reconstruction from URA II as the coding system with URA I as the decoding system, photographically reversed to correct for black correlation spot.

Fourth Row: Extreme left. Input object of a spoked system. Other reconstructions of this object as for Row 3.

Fifth Row : Extreme left. Input object resembling a Picker Phantom. Other reconstructions of this object as for Row 3.

Fig 6·6·1

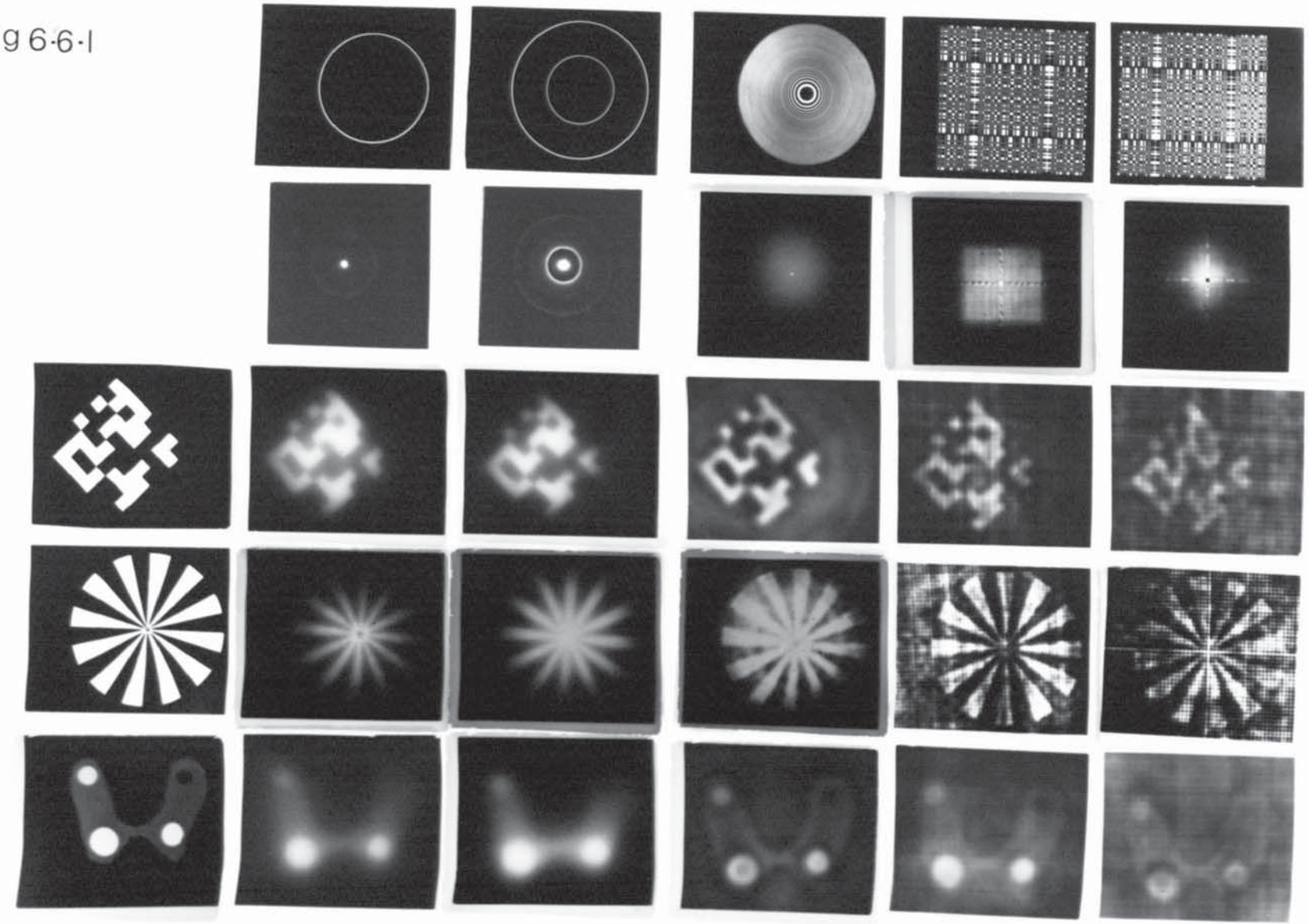

CHAPTER 7

TOMOGRAPHICAL POSSIBILITIES

CHAPTER 7

TOMOGRAPHICAL POSSIBILITIES

7.1 INTRODUCTION TO TOMOGRAPHY

Tomography has been one of the promised benefits of Coded Aperture Imaging since the technique was developed by Mertz and Young[5]. Several authors have reported the use of Fresnel Zone Plates, Random Arrays, Nonredundant Point Arrays and the Annulus, for tomographic work. Chang et al.[24] have compared the tomographic possibilities by analysing the System-Point-Spread-Functions (SPSFs) for various coded apertures subject to various decoding methods and concluded that the Random Array offered best results.

Recently, Cannon and Fenimore[55] have compared the Random Array with a Uniformly Redundant Array (URA) for point source objects and concluded that a URA based on m-sequences[59] provided better images than those obtained using Random Arrays. More recently, Kujoory et al.[79] have used a time-variant aperture to perform tomography. Once more results of 'dilute' objects are presented.

We use extended objects and compare the performances of the Twin Annulus and the URAs, both m-sequence based and the quadratic residue type.

In the next section we consider the mathematical preliminaries needed in the analysis of tomographic images.

7.2 THEORY

Let us consider a three dimensional object $O(x,y,z)$ and let the coded aperture be represented by $A(p,q)$. Assuming the system to be space-invariant and linear, the coded picture, $G(u,v)$, of the nth layer of the object along the z-direction at a distance z_n is given by the convolution of the object, suitably scaled, with the intensity PSF of the coded aperture.

Thus,

$$G(u,v) = \sum_{n=1}^{m} \{k_n O_n(x,y) \circledast\circledast (1+k_n)A(p,q)\} \qquad (7.2.1)$$

where $\circledast\circledast$ represents a two dimensional convolution
a,b are the object to code and code to detector distances respectively. k is the ratio (b/a).

The reconstruction $I(x,y,z)$ is performed by correlating the coded picture with the original code (coded aperture).

$$I(x,y,z) = \sum_{n=1}^{m} \{G(u,v) * * A(p,q)\} \qquad (7.2.2)$$

where $G(u,v)$ contains depth information implicit in Eqn. (7.2.1).

Now

$$I(x,y,z) \approx \sum_{n=1}^{m} I_n(x,y) \qquad (7.2.3)$$

If the coded picture is illuminated by noncoherent light, the irradiance immediately behind it is

$$I = I_o G(u,v)$$

where I_o is the irradiance at the plane of the coded picture.

By substituting for G(u,v) in Eqn (7.2.2) and re-arranging we find that by placing a photographic film at a distance z_n from the coded aperture, it records.

$$I_n(x,y) = I_o \Big| \{A(p,q) ** A(p,q)\} \circledast\circledast O_n(x,y) + \sum_{\substack{j=1 \\ j\neq n}}^{m} \frac{k_n}{k_j} O_j(x,y) \circledast\circledast \{\frac{(1+k_n)}{(1+k_j)} A(p,q) ** A(p,q)\} \Big| \qquad (7.2.4)$$

where ** is two dimensional correlation.

If

$$\{A(p,q) ** A(p,q)\} = \delta(x,y) \qquad (7.2.5)$$

i.e. a delta function

Then Eqn. (7.2.4) becomes

$$I_n(x,y) = I_o O_n(x,y) + \text{2nd term of Eqn (7.2.4)} \qquad (7.2.6)$$

This 2nd term of Eqn. (7.2.4) will produce out-of-focus effects.

This is because

$$A(p,q) ** \frac{(1+k_n)}{(1+k_j)} A(p,q)$$

i.e. the correlation of the intensity PSF of the coded aperture for the nth layer with the PSFs of all other layers does not produce a uniform d.c. background or a uniform field of zeros in digital correlation.

So, ideally, there would only be out-of-focus effects making a contribution to the overall "d.c." background. The randomness of the coded aperture is likely to reduce the unwanted cross-correlation terms producing these out-of-focus effects (Chang et al.[24], Fenimore and Cannon[55]).

On the other hand, if $k_n >> k_j$ then the cross-correlation terms will also be reduced but at the expense of adverse depth resolution, inverse square law effects and undesirable Lambertian effects on the coded picture.

If however, $A(p,q)**A(p,q) \neq \delta(x,y)$ is not a delta function, artifacts are also introduced into the reconstructed image.

The reconstruction will then be the convolution of the object with this nonideal autocorrelation of the coded aperture.

In this case we have artifacts, due to the nonideal nature of the autocorrelation function of the code, as well as the out-of-focus effects both making a contribution to the overall "d.c." background.

7.3 OPTICAL SIMULATION

We prepared our codes and objects as transparencies on Kodalith ortho type 3 (2556) film. The Twin Annulus was constructed with mean inner radius R_1=8mm and outer radius R_2=24mm with the annular width w=0.45mm. Both URAs were mosaic versions of the basic r×s pattern. For the URA based on quadratic residues r=61 and s=59, with w the mean cell dimension = 0.42mm. For the m-sequence URA, r=65 and s=63, with w=0.42mm. For coding a 2r×2s mosaic was used in each case.

Tomography was simulated by using two extended planar objects separated by 30mm and subjecting the coded picture to successive exposures. The 'square' object was determined by a sequence of random numbers - even numbers in this sequence giving rise to transparent squares and odd to opaque squares. This 19mm square object consisted of 64 unit cells out of which ~ 50% were clear and hence transmitting. The sppke target was 34mm in diameter, Fig. 7.4.2.

The objects were placed 120mm and 150mm away from the code and the plane of the coded picture lay 100mm away from the code. Fig. 7.3.1. The coded pictures were recorded on Ilford ortho (SP348) film and processed to give a contrast index of 0.7 in Ilford ID-11 developer. The exposure of the Twin Annulus was incremented by a factor dependent on the relative transmissions of the Twin Annulus and URA. Thus the Twin Annulus received an exposure ×14 the URA exposure.

Decoding was performed by correlating the coded picture with the original code having made a contact print of the

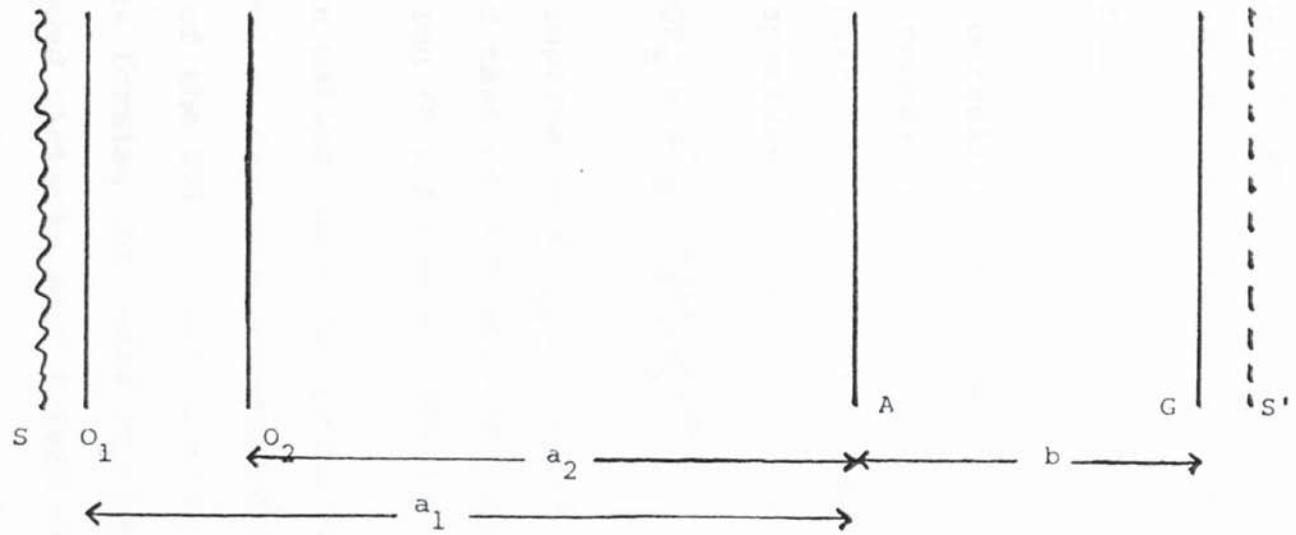

Fig.7.3.1 Coding and decoding configuration in Tomography simulations.

O_1 = Object transparency (34mm spoke target)

O_2 = Object transparency (19mm square object)

S = diffuse source ; A = coded aperture plane ; G = coded picture plane

S' = position of source in decoding

former described in Chapter 5.

In the case of the URAs, the coded picture was masked by an aperture mr×ms, where

$$mr \times ms = \left|\{(k+1)(r \times w)\} + \frac{d}{2}k\right| \times \left|\{(k+1)(s \times w)\} + \frac{d}{2}k\right|$$

before correlation with the original code. Since the coding process is a convolution, an inversion of π radians takes place. Thus decoding was performed by inverting the coded aperture. From Eqn (5.5.2) Chapter 5, we note that

$$DQE_E \alpha \frac{(\text{contrast})^2 \times \text{Speed}}{\text{Granularity}}$$

which implies $(S/N)_{out} \alpha \text{ contrast}(\gamma_E)$.
We find that contact printing only causes a negligible reduction in the overall DQE transfer, see Chapter 5.

In making our coded pictures the Twin Annulus received an exposure corresponding to the transmission ratio of the URA to Twin Annulus. Thus the number of photons forming the coded picture is comparable. All the coded pictures were formed on Ilford ortho (SP348) film and developed to give a contrast index (γ_E) of 0.7.

Thus we simulate photon shot noise in γ-ray imaging by the photographic grain noise in the manner of Rogers et al.[12] in the coding process. Films used for contact printing and recording reconstructions are of course different, this being determined by the nature of the SPSFs.

7.4 Results and Conclusions

For convenience the results are tabulated in Fig. 7.4.1. The top row show the coded apertures simulated. The second row illustrates the nature of the undesirable SPSFs of these apertures under a noncoherent correlation decoding system. The first column of the third and fourth rows show the objects encoded. Adjacent to these objects lie the reconstructions from the various coded apertures, placed in the column directly below each aperture..

The Twin Annulus reconstructions show the $\frac{1}{r}$ variation in the shoulder of the SPSF artifact and the artifacts introduced by the 2^{nd} term of Eqn. (7.2.4), the latter being responsible for out-of-focus behaviour. Clearly, the cross-correlation terms from the out-of-focus planes contribute significantly and as a result the Twin Annulus, whilst useful for planar objects, does not fulfil tomographic expectations.

The URA based on quadratic residues shows the artifacts introduced to the SPSF in noncoherent correlation decoding but also shows artifacts introduced as a result of the 2^{nd} term of Eqn. (7.2.4). These cross-correlation terms from out-of-focus planes, probably due to the symmetrical nature of this URA, have a detrimental effect on spatial resolution.

The URA based on m-sequences, whilst exhibiting the nonideal SPSF inherent in our decoding system, is relatively exempt from artifacts from the 2^{nd} term of Eqn. (7.2.4).

This is attributed to the more random nature of this URA[55]. Instead, there is a uniform increase in the 'd.c.' background expected as a result of the zero cross-correlation terms.

The intensity variation present in the URA reconstructions is as a result of the off-axis projection of the image, due to inversion of the code in the decoding process. This is somewhat exaggerated by the high contrast index of the recording film.

We conclude that the URA based on m-sequences possess good spatial resolution and out-of-focus behaviour characteristics. It is capable of imaging extended objects and should be the coded aperture to realise tomographic possiblities. This complements the results of Cannon and Fenimore[55] who successfully decoded point source objects with this type of URA.

FIG. 7.4.1 PERFORMANCE OF THE CODED APERTURES UNDER TEST FOR THEIR TOMOGRAPHIC CAPABILITIES

Top Row : Aperture codes L to R Twin Annulus, URA (quadratic residue), URA (m-sequence).

Second Row: Items 1-3 autocorrelations of the coded apertures.

Third Row : Extreme left. Input object of squares derived from a set of random numbers placed 120mm from coded aperture. Items 1-3 reconstruction of this object using the codes at the top.

Fourth Row: Extreme left. Input object of a spoke target placed 150mm from the coded aperture. Other reconstructions of this object as for row 3.

Fig 7-4-1

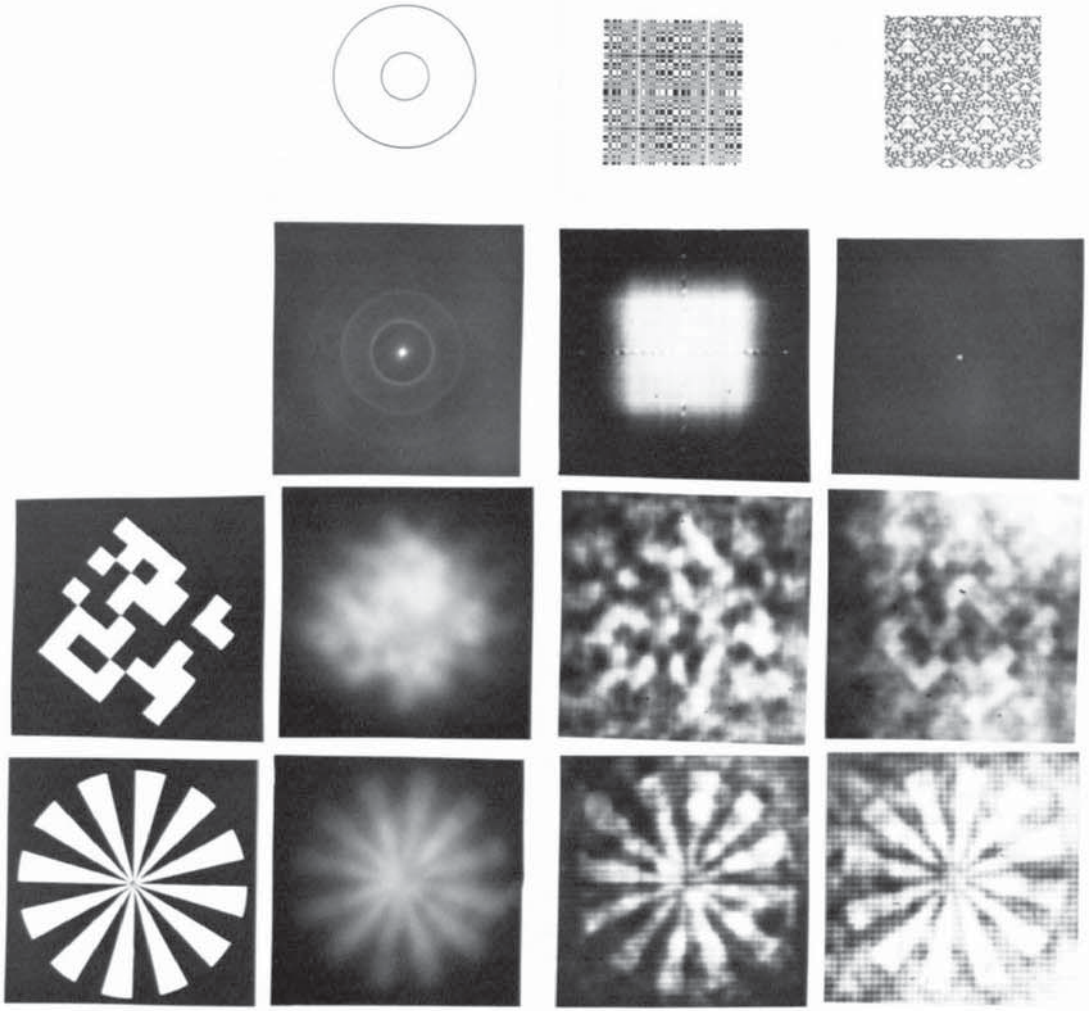

CHAPTER 8

CONCLUSIONS

CHAPTER 8

CONCLUSIONS

We have compared by optical simulation the relative performances of various coded apertures subject to a noncoherent optical decoding technique. Extended and continuous tone planar objects have been coded and decoded using the Annulus, Twin Annulus, Fresnel Zone Plate and the Uniformly Redundant Array.

We have also compared the tomographic capabilities of the Twin Annulus with the Uniformly Redundant Arrays based on quadratic residues and m-sequences. The simulation was performed by using two planar objects separated by a distance of 30 mm and recording the convolution of each object with the coded aperture on the same film.

The decoding technique we have used is one of noncoherent optical correlation. This basically involves correlating the coded picture with the original coded aperture.

The System-Point-Spread-Function (SPSF) or autocorrelation of the coded aperture determines the nature of the reconstructed image. For the Annulus and Twin Annulus, the SPSF, under noncoherent correlation, is characterised by a $\frac{1}{r}$ shoulder on the autocorrelation peak. The Fresnel Zone Plate, under such a decoding system, is characterised by a "ringing" effect. The

Uniformly Redundant Arrays subject to a noncoherent correlation decoding system possesses undesirable artifacts not present in digital correlation.

Thus all the coded apertures simulated possess an undesirable SPSF when subject to our noncoherent correlation system of decoding. In an ideal situation this SPSF will be a Dirac-delta-function. Of course when decoding point source or dilute objects the effects of the undesirable SPSF can be minimized and with certain coded apertures - eliminated. However, when decoding extended and continuous -tone objects, the reconstruction is degraded by the effects of the undesirable SPSF. The reconstruction is said to contain artifacts. The results of decoding extended and continuous-tone planar objects, illustrating these artifacts using the coded apertures under test are shown in Fig. 6.6.1.

The results of the tomographic capabilities of the Twin Annulus and URAs are presented in Fig. 7.4.1. In addition to the $\frac{1}{r}$ intensity variation in the shoulder of the SPSF artifact, this coded aperture also has undesirable out-of-focus properties. Although it is possible to circumvent the $\frac{1}{r}$ intensity variation by digital means, it is envisaged that the background (contribution from all out-of-focus planes) from several planes, as opposed to the two planes simulated, will seriously degrade the reconstruction from the selected plane.

Of the two types of URAs simulated the one based on quadratic residues contains more out-of-focus artifacts than the URA based on m-sequences. As a result of this, the spatial resolution in the reconstructions is greatly impaired. Again, it is possible to obtain an artifact-free SPSF by digital correlation techniques however, artifacts will be introduced by the out-of-focus behaviour of this coded aperture.

The URA based on m-sequences is relatively exempt from out-of-focus behaviour and whilst exhibiting a non-ideal SPSF is better than that of other codes.

This is attributed to the more "random" nature of this type of URA. Instead there is a uniform increase in the "d.c." background expected as a result of the zero cross-correlation terms. The reconstructions also show the excellent spatial resolution capability of this coded aperture. It is envisaged that digital correlation techniques applied to this coded aperture will yield excellent tomographic images of extended objects.

REFERENCES

REFERENCES

1. G. L. Rogers, "Gabor diffraction microscopy: the hologram as a generalised zone plate"
   Nature (GB) 116, 237, 1950.

2. G. L. Rogers, "The black and white hologram"
   Nature (GB) 166, 1027, 1950.

3. G. L. Rogers, "Experiments in diffraction microscopy"
   Proc. Roy. Soc. (Edinburgh) A63, 193-221, 1952.

4. G. L. Rogers, "Artificial holograms and astigmatism"
   Proc. Roy. Soc. (Edinburgh) A63, 313-325, 1952.

5. L. Mertz and N. O. Young, "Fresnel transformation of Images"
   Proceedings of the International Conference on Optical Instruments, London, 305-312, 1961.

6. N. O. Young, "Photography without lenses or mirrors"
   Sky Telesc. 25, 8-9, 1963.

7. H. H. Barrett, "Fresnel zone plate imaging in nuclear medicine"
   J. Nuc. Med. 13, 382-385, 1972.

8. H. H. Barrett, D. T. Wilson and G. D. De Meester, "The use of half tone screens in Fresnel zone plate imaging of incoherent sources"
   Opt. Commun. 5, 398-401, 1972.

9. W. L. Rogers, K. S. Han, L. W. Jones and W. H. Beierwaltes, "Application of a Fresnel zone plate to gamma ray imaging"
J. Nuc. Med. 13, 612-615, 1972.

10. H. H. Barrett, K. Garewal and D. T. Wilson, "A spatially coded X-ray source"
Radiology 104, 429-430, 1972.

11. D. T. Wilson, G. D. De Meester, H. H. Barrett and E. Barsack, "A new configuration for coded aperture imaging"
Opt. Commun. 8, 384-386, 1973.

12. W. L. Rogers, L. W. Jones and W. H. Beierwaltes, "Imaging in nuclear medicine with incoherent holography"
Opt. Eng. 12, 13-22, 1973.

13. H. J. Caulfield and A. D. Williams, "An introduction to holography by shadow casting"
Opt. Eng. 12, 3-7, 1973.

14. H. H. Barrett, D. T. Wilson, G. D. De Meester and H. Scharfman, "Fresnel zone plate imaging in radiology and nuclear medicine"
Opt. Eng. 12, 8-12, 1973.

15. H. H. Barrett and F. A. Horrigan, "Fresenel zone plate imaging of gamma rays: theory"
Appl. Opt. 12, 2684-2702, 1973.

16. M. D. Tipton, J. E. Dowdy and H. J. Caulfield, "Coded aperture imaging with on-axis Fresnel zone plates" Opt. Eng. 12, 166-168, 1973.

17. A. G. Lingren, D. K. Guha and J. E. Spence, "A noise analysis of Fresnel zone plate imaging systems" Proceedings of the International Optical Computing Conference, Zurich, New York: IEEE No. 74CHO 862-3C, 54-59, 1974.

18. H. H. Barrett, W. W. Stoner, D. T. Wilson and G. D. De Meester, "Coded apertures derived from the Fresnel zone plate" Opt. Eng. 13, 539-549, 1974.

19. R. Silva and G. L. Rogers, "Decoding of a noncoherent hologram in noncoherent light" J. Opt. Soc. Amer. 65, 1448-1450, 1975.

20. D. R. Dance, B. C. Wilson and R. P. Parker, "Digital reconstruction of point sources imaged by a zone plate camera" Phys. Med. Biol. 20, 747-757, 1975.

21. B. C. Wilson, R. P. Parker and D. R. Dance, "Digital processing of images from a zone plate camera" Phys. Med. Biol. 20, 757-770, 1975.

22. M. H. Farmelant, G. D. DeMeester, D. T. Wilson and H. H. Barrett, "Initial clinical experiences with a Fresnel zone plate imager" J. Nuc. Med. 16, 183-187, 1975.

23. T. F. Budinger and B. Macdonald, "Reconstruction of the Fresnel-coded gamma camera images by digital computer"
J. Nuc. Med. 16, 309-313, 1975.

24. L. T. Chang, B. Macdonald and V. Perez-Mendez, "Comparisons of coded aperture imaging using various apertures and decoding methods"
Applications of Optics in Medicine and Biology, edited by T. Hirschfield and R. E. Herron, SPIE Proceedings Vol. 89, (Bellingham: Society of Photo-optical Instrumentation Engineers), 9-16, 1976.

25. R. Silva and G. L. Rogers, "Coded aperture imaging - a noncoherent optical approach"
Accepted for publication in Optica Acta February 1981.

26. G. L. Rogers "A new method of analysing ionospheric movement records"
Nature (London), 177, 613-4, 1956.

27. E. N. Leith and J. Upatnieks, "Reconstructed wave fronts and communication theory"
J. Opt. Soc. Amer. 52, 1123-1130, 1962.

28. G. L. Rogers, *Noncoherent Optical Processing*, New York: Wiley, Ch. 7, 1977.

29. R. H. Dicke, "Scatter-hole cameras for x-rays and gamma rays"
Astorphys. J. 153, L101-L106, 1968.

30. R. L. Blake, A. J. Burek and E. E. Fenimore, "Solar x-ray photography with multiplex pinhole camera"
Rev. Sci. Instrum. 45, 513-516, 1974.

31. L. T. Chang, S. Kaplan and B. Macdonald, "A method of tomographic imaging using a multiple pinhole coded aperture"
J. Nuc. Med. 15, 1063-1065, 1974.

32. L. Alquazzaz and G. L. Rogers, "Coding and decoding of dilute and continuous-tone objects in incoherent light"
J. Opt. Soc. Amer. 65, 695-699, 1975.

33. A. Z. Akcasu, R. S. May, G. F. Knoll, W. L. Rogers, K. F. Koral and L. W. Jones, "Time modulated coded apertures for γ-ray imaging in nuclear medicine"
Proceedings of the International Optical Computing Conference, Zurich, New York, IEEE No. 74, CHO 862-3C, 49-53, 1974.

34. R. S. May, A. Z. Akcasu and G. F. Knoll, "γ-ray imaging with stochastic apertures"
Appl. Opt. 13, 2589-2601, 1974.

35. A. Macovski, "Gamma ray imaging system using modulated apertures"
Phys. Med. Biol. 19, 523-533, 1974.

36. K. F. Koral, W. L. Rogers and G. F. Knoll, "Digital tomographic imaging with time-modulated pseudorandom coded aperture and Anger camera"
J. Nuc. Med. 16, 402-423, 1975.

37. M. J. E. Golay, "Point arrays having compact non-redundant autocorrelations"
J. Opt. Soc. Amer. 61, 272-273, 1971.

38. A. Wouters, K. M. Sunion and J. G. Hirschberg, "Direct method of dedoding multiple images"
Appl. Opt. 12, 1871-1873, 1973.

39. E. Klotz and H. Weiss, "Three dimensional coded aperture imaging using nonredundant point distributions"
Opt. Commun. 11, 368-372, 1974.

40. E. Klotz, R. Linde and H. Weiss, "A new method for deconvoluting coded aperture images of three-dimensional x-ray objects"
Otp. Commun. 12, 183-187, 1974.

41. W. K. Klemperer, "Very large array configurations for the observation of rapidly varying sources"
Astron. Astrophys. Suppl. 15, 449-451, 1974.

42. H. Weiss, "Three-dimensional x-ray information retrieving by optical filtering"
Proceedings of the International Optical Computing Conference, Zurich, New York, IEEE No. 74, CHO 862-3C, 41-44, 1974.

43. P. Chavel and S. Lowenthal,"Noise and coherence in optical image processing I: The Callier effect and its influence on image contrast"
J. Opt. Soc. Amer. 68, 559-568, 1978.

44. P. W. Walton, "An aperture imaging system with instant decoding and tomographic capabilities"
J. Nuc. Med. 14, 861-863, 1973.

45. J. Fonroget, Y. Belvaux and S. Lowenthal,"Fonction de transfert de modulation d'un systeme de gammagraphie holographique"
Opt. Commun. 15, 76-79, 1975.

46. R. G. Simpson, H. H. Barrett, J. A. Subach and H. D. Fisher, "Digital processing of annular coded aperture imagery"
Opt. Eng. 14, 490-494, 1975.

47. J. Brunol and J. Fonroget, "Bruit Multiplex en gammagraphie par codage"
Opt. Commun. 22, 301-306, 1977.

48. J. Brunol, J. Fonroget and S. Lowenthal, "Déconvolution analogique en imagerie par ouverture codée appliquée à la médecine nucléaire"
Opt. Acta 25, 113-124, 1978.

49. J. Brunol, N. de Beaucoudray, J. Fonroget and S. Lowenthal, "Qualitative and quantitative images with coded apertures"
Optica Hoy y Manana, Proceedings of the Eleventh Congress of the International Commission for Optics, ICO-11, Madrid, 199-201, 1978.

50. R. Silva and G. L. Rogers, "Coding and decoding pictures in nuclear medicine"
To be published in Pattern Recognition, 1981.

51. M. E. Haine and T. Mulvey, "The formation of the diffraction image with electrons in the Gabor diffraction microscope"
J. Opt. Soc. Amer. 42, 763-773, 1952.

52. E. E. Fenimore and T. M. Cannon, "Coded aperture imaging with uniformly redundant arrays"
Appl. Opt. 17, 337-347, 1978.

53. E. E. Fenimore, "Coded aperture imaging: predicted performance of uniformly redundant arrays"
Appl. Opt. 17, 3562-3570, 1978.

54. E. E. Fenimore, T. M. Cannon and E. L. Miller, "A comparison of Fresnel zone plates and uniformly redundant arrays"
Applications of Digital Image Processing, SPIE Proceedings Vol. 149, (Bellingham: Society of Photo-optical Instrumentation Engineers) 232-236, 1978.

55. T. M. Cannon and E. E. Fenimore, "Tomographical imaging using uniformly redundant arrays" Appl. Opt. 18, 1052-1057, 1979.

56. E. E. Fenimore, "Coded aperture imaging: the modulation transfer function for uniformly redundant arrays" Appl. Opt. 19, 2465-2471, 1980.

57. D. Calabro and J. K. Wolf, "On the synthesis of two-dimensional arrays with desirable correlation properties" Inform. Control 11, 537-560, 1968.

58. F. J. MacWilliams and N. J. A. Sloane, "Pseudo-random sequences and arrays" Proc. IEEE 64, 1715-1729, 1976.

59. G. F. Gunson and B. Polychronopulos, "Optimum design of a coded mask x-ray telescope for rocket applications" Mon. Not. R. Astron. Soc. 177, 458-497, 1976.

60. L. J. Cutrona, E. N. Leith, C. J. Palermo and L. J. Porcello, "Optical data processing and filtering systems" IRE Trans. Inform. Theory, Vol. IT-6, 386-400, 1960.

61. A. Vander Lugt, "A review of optical data-processing" Opt. Acta. 15, 1-33, 1968.

62. J. W. Goodman, *Introduction to Fourier optics*, New York: McGraw-Hill, Ch. 7, 1968.

63. A. R. Shulman, *Optical data processing*, New York: Wiley, 1970.

64. K. Preston, *Coherent optical computers*, New York: McGraw-Hill, 1972.

65. F. T. S. Yu, *Introduction to diffraction, information processing and holography*, Cambridge MA; M.I.T. Press, Ch. 7, 1973.

66. A. Vander Lugt, "Coherent optical processing" Proc. IEEE 62, 1300-1319, 1974.

67. M. A. Monahan, K. Bromley and R. P. Bocker, "Incoherent optical correlators" Proc. IEEE 65, 121-129, 1977.

68. G. L. Rogers, "Noncoherent optical processing" Optics and Laser Technology 7, 153-162, 1975.

69. G. L. Rogers, *Noncoherent optical processing*, New York: Wiley, 1977.

70. G. L. Rogers, "Incoherent optical methods for selecting and pre-processing information for analogue and digital computers" Proc. Technical Programme Electro-Optical Systems Design Conference, New York, 8-19, 1970.

71. E. L. O'Neill, *Introduction to statistical optics*, Reading Mass; Addison-Wesley, 1963.

72. R. E. Jackson, (Ed), *The manual of photography*, Focal Press: London and New York, Ch. 15, 1978.

73. J. C. Dainty and R. Shaw, *Image science*, Academic Press: London, 1976.

74. W. L.Bragg and G. L. Rogers, "Elimination of the unwanted image in diffraction microscopy" Nature (GB) 167, 190, 1951.

75. I. Leifer, G. L. Rogers and N. W. F. Stephens, "Incoherent Fourier transformation: a new approach to character recognition" Opt. Acta. 16, 535-553, 1969.

76. N. W. F. Stephens and G. L. Rogers, "The Fourier transformer" Physics Education (London), 9, 331-334, 1974.

77. G. L. Rogers, "Qualitative and semi-quantitative Fourier transformation using a noncoherent system" Appl. Opt. 18, 3152-3155, 1979.

78. G. L. Rogers, "Noncoherent methods of Fourier transformation" Proc. Int. Opt. Comp. London, S. Horwitz (Ed.), IEEE New York, No. 78CH 1305-2C, 169-171, 1979.

79. M. A. Kujoory, E. L. Miller, H. H. Barrett, G. R. Gindi and P. N. Tamura, "Coded aperture imaging of γ-ray source with an off-axis rotating slit" Appl. Opt. 19, 4186-4195, 1980.